

Testing of combined Mn/Si oxygen carriers supported on CaO or Al_2O_3 for converting methane and syngas

Baoyi Wang

Department of Chemistry and Chemical Engineering
Division of Environmental Inorganic Chemistry
CHALMERS UNIVERSITY OF TECHNOLIGY
Göteborg, Sweden 2017

Testing of combined Mn/Si oxygen carriers supported on CaO or Al_2O_3 for converting methane and syngas

Wang Baoyi

© Wang Baoyi

Supervisor: Henrik Leion, Chalmers University of Technology

Examiner: Henrik Leion, Chalmers University of Technology

Department of Chemistry and Chemical Engineering
Division of Environmental Inorganic Chemistry
SE- 412 96 Göteborg
Sweden
Telephone: +46 (0) 70 404 26 55

Testing of combined Mn/Si oxygen carriers supported on CaO or Al_2O_3 for converting methane and syngas

Department of Chemistry and Chemical Engineering
Environmental Inorganic Chemistry Division
Chalmers University of Technology, Göteborg, Sweden

Abstract:
Facing increasingly severe environmental problems and substantial energy demand, chemical-looping with oxygen uncoupling (CLOU) is regarded as a highly promising technique to facilitate the application of carbon capture and storage (CCS) due to its low cost and inherent gas separation. Thus, feasible oxygen carriers for the continuous operation in industry scale are essential. The combination of Mn and Si, which is not only economic but also has low adverse effect on the environment, has been tested to be able to provide satisfactory CLOU behavior. However, the mechanical properties require further improvement. Hence, two kinds of support materials are chosen in this study i.e. CaO and Al_2O_3 to enhance physical strength of the Mn-Si oxides. Twelve samples with a CaO content ranging from 2wt% to 41wt% and twelve samples with a Al_2O_3 content varying in the range of 2wt% and 36wt% are produced using spray-drying at three sintering temperatures i.e. 1100 °C, 1150°C and 1200 °C. The aim is to identify the most practical oxygen carrier which exhibits high reactivity and strong mechanical characteristics. The oxygen release ability and gas fuel conversion are examined. In general, the particles with lower support materials' content (≤ 5wt%) calcined from lower temperatures (≤1150°C) show better CLOU behavior and higher reactivity, regardless of the support material. Oxygen carriers supported by Al_2O_3 suffer deactivation after undergoing the strongest operation condition (1050°C). In addition, the attrition resistance, crushing strength and crystalline phase composition are also assessed to determine the best candidates.

Keywords: chemical-looping combustion (CLC), chemical-looping with oxygen uncoupling (CLOU), manganese-silicon oxides, supporting material

Category

1. INTRODUCTION 1

1.1 CHEMICAL-LOOPING COMBUSTION (CLC) 1

1.2 CHEMICAL LOOPING WITH OXYGEN UNCOUPLING (CLOU) 2

1.3 OXYGEN CARRIERS 2

1.4 OBJECTIVE 4

2. EXPERIMENTAL 5

2.1 ASSESSED OXYGEN CARRIERS 5

2.2 EXPERIMENTAL METHOD AND SETUP FOR REACTIVITY TEST 6

2.3 DATA EVALUATION 9

2.4 CHARACTERIZATION OF MATERIALS 10

3. RESULTS 11

3.1 CLOU PROPERTIES (OXYGEN RELEASE) 11

3.2 REACTIVITY TEST 14

3.2.1 Fuel gas conversion capacity of Mn-Si oxides supported on CaO 14

3.2.2 Fuel gas conversion capacity of Mn-Si oxides supported on Al_2O_3 16

3.3 MECHANICAL PROPERTIES 19

3.4 X-RAY DIFFRACTION RESULTS 22

3.5 ELECTRON IMAGES (SEM) 23

4. CONCLUSIONS 27

5. REFERENCE 28

6. APPENDIX 31

6.1 CLOU OXYGEN RELEASE 31

6.2 FUEL CONVERSION 34

6.3 MECHANICAL DURABILITY 47

1. Introduction

One of the most severe problems during the recent decades is the greenhouse effect. Even a slight rise in global temperature could engender catastrophic climate changes (Lenton, 2011). The main contributor among the greenhouse gases is carbon dioxide. One third of carbon dioxide is estimated to be emitted from fossil fuel combustion to produce energy (Jabbary, 2014). Thus, this human activity is regarded as the principal contributor to the global warming. Although various renewable energy techniques have already been developed to generate power in order to mitigate the global warming, it will still take some time before they can satisfy the intensive energy demand. Based on this fact, energy produced from combustion of fossil fuels will still dominate the worldwide energy market in the short term, which proposes a high requirement for the control of CO_2 emissions. To reach this aim, different technologies are suggested, and among them, carbon capture and storage (CCS) is one of the most promising alternatives.

Since more or less undiluted CO_2 is essential to ensure the feasibility of CCS, several paths to separate CO_2 have been proposed and investigated, such as pre-combustion, oxy-fuel combustion and post-combustion (Toftegaard, 2010) (Kanniche, 2010). However, these techniques are always accompanied with great energy penalty. In this term, chemical-looping combustion (CLC) with efficient power generation, low energy consumption and low adverse environmental impacts attracts great attention in the energy field (Fan, 2016).

1.1 Chemical-looping combustion (CLC)

In CLC process, a metal oxide or a combination of metal oxides is circulated between inter-connected dual fluidized beds (Fig. 1). The metal oxide, which is usually referred to as oxygen carrier, is applied as bed material to provide oxygen for the combustion of injected fuel in the fuel reactor, shown in Eq.1. The reduced oxygen carrier is then transferred back to the air reactor for regeneration, shown in Eq.2 (Mohammad Pour, 2013). It can be found that the net reaction happening in the CLC combustion is the same as that in the conventional one, which indicates the CLC system release the same amount of heat as that in the common one (Mattisson, 2009).

In the fuel reactor reaction Eq.1 takes place.

$$(2n + m)Me_xO_y + C_nH_{2m} \rightarrow (2n + m)Me_xO_{y-1} + mH_2O + nCO_2 \qquad \text{Eq.1}$$

In the air reactor reaction Eq.2 takes place.

$$2Me_xO_{y-1} + O_2 \leftrightarrow 2Me_xO_y \qquad \text{Eq.2}$$

In CLC, CO_2 and H_2O with a little amount of impurities are intrinsically separated from the nitrogen and residual oxygen originating from the combustion air. Since elimination of water vapor can be easily achieved by condensation, the exhaust gas from the combustion consists of almost pure carbon dioxide (Lyngfelt, 2001). Thus, CLC is thought to be one promising carbon capture technique which can obtain pure CO_2 without large energy usage and extra expensive gas separation (Siriwardane, 2015). This superiority over other techniques also occurs in chemical looping with oxygen uncoupling (CLOU), which will be described later.

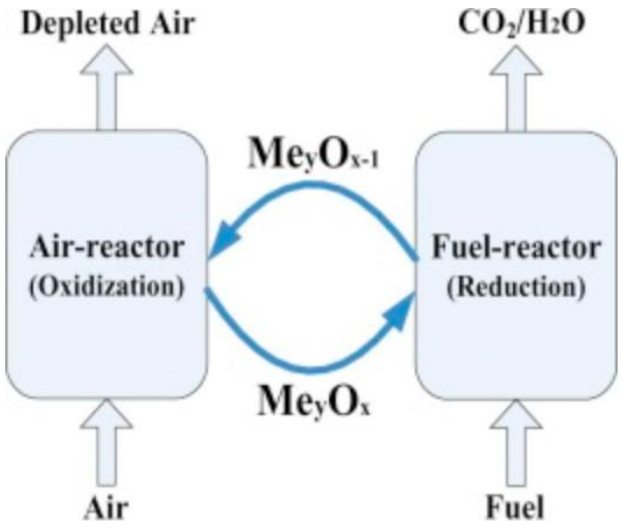


Fig. 1. Schematic representation of the chemical-looping combustion process (Ge, 2016).

1.2 Chemical looping with oxygen uncoupling (CLOU)

Due to the capacity of some metal oxides to release oxygen spontaneously under inert atmospheric condition, CLOU systems are developed to facilitate the utilization of solid fuels, described by Eq.3 to Eq.6 (Keller, 2014). Although the total reactions in both combustion systems (CLC and CLOU) are the same, the mechanisms to oxidize the fuel are different. Solid-phase fuel has to be gasified to be able to react with the oxides which is also solid in conventional CLC system. However, in CLOU, the oxygen released by the oxidized oxygen carriers reacts with the fuel in solid-phase directly as well as gas-phase in the fuel reactor (Rydén, 2014). The depleted oxygen carriers are then circulated to air reactor to capture oxygen again. In the case of solid fuels, previous studies also demonstrate that compared with normal CLC, which depends on a slow gasification step, the speed of coke oxidation rises at least an order of magnitude when using CLOU system (Leion, 2009). Hence, this more efficient system consumes less oxygen carriers and scales down the reactor size resulting in less costs (Mattisson, 2009).

In the fuel reactor reactions Eq.3, Eq.4 and Eq.5 occur.

$$Me_xO_y \leftrightarrow M_xO_{y-2} + O_2(g) \qquad \text{Eq.3}$$

$$C_nH_{2m} + (n + \frac{m}{2})O_2(g) \rightarrow mH_2O + nCO_2 \qquad \text{Eq.4}$$

$$C + O_2(g) \rightarrow CO_2 \qquad \text{Eq.5}$$

In the air reactor reaction Eq.6 occurs.

$$Me_xO_{y-2} + O_2(g) \leftrightarrow Me_xO_y \qquad \text{Eq.6}$$

1.3 Oxygen carriers

One of the main concerns of both CLC and CLOU systems is the bed material, which has a critical effect on the whole operation. Oxygen carriers are supposed to maintain high reaction rates and transport capacity in long-term operation (Zhao, 2012). Economic factors and mechanical durability as well as absence of agglomeration are also significant aspects in the choice of the oxygen carrier materials. Any threat that metal oxides exert on the surroundings should be considered as well (Tian, 2010). Furthermore, combustions of different fuels have their own specific requirements. When combusting gas-phase fuels, it might be beneficial to

apply bed materials with higher price since the cost of elimination of unwanted impurities is reasonable. However, with respect to ash-containing combustibles, cheaper materials are more suitable since they require frequent replacement (Lyngfelt, 2014). In general, materials' choice is a trade-off between life span and price. Moreover, in CLOU system, oxygen carriers should be able to react reversibly with O_2. They should provide adequate gaseous O_2 in the fuel reactor and be regenerated to the initial state by the combustion air in the air reactor (Shulman, 2011). This capability is determined by the equilibrium oxygen partial pressure at definitive temperature, which is various for various materials (Rydén, 2014).

In recent years, substantial experiments have been conducted on different materials based on Mn, Ni, Cu and Fe as well as other mixed metal oxides (Adanez, 2012).

One of the extensively investigated groups of materials are Cu-based materials. Unfortunately, their natural properties are the obstacles in the application in the industrial-scale CLC processes. One limitation is that the allowed temperature when using these materials might be too low to reach the demand of combustion. It is known that the copper has relatively low melting temperature (1085 °C). High reduction of copper-based materials to metallic copper might occur in the strong combustion conditions. Thus, the bed materials are more likely to agglomerate since combustion requires high temperature (Zhao, 2012). Besides, it might not be economically feasible to use Cu-based materials due to their relatively high costs (Frick, 2016). Combination with an apt support material could be a viable manner to deal with the agglomeration. Copper-based materials supported by Al_2O_3 with addition of NiO have proven to exhibit stable behavior at high temperatures (1173 K in the fuel reactor and 1223 K in the air reactor) for a rather long time (Pilar Gayán, 2011).

Another type of interesting candidates is Ni-based oxygen carrier with high reactivity, which might be related to the catalytic characteristic of nickel. $NiO/NiAl_2O_4$-oxygen carriers have been tested to exhibit noteworthy efficiency (around 98%) for more than 1000-h operation with no deactivation (Linderholm, 2009). However, the sensitivity of NiO-based oxygen carriers to sulphur poisoning prevents them from converting fuel containing sulphur (García-Labiano, 2009). Additionally, shortened life span caused by the possible substantial losses when combusting ash-containing fuels as well as the high cost of the raw materials make nickel less attractive (Leion, 2009). Thus, their application is then limited to the reaction of gaseous and ash-free combustibles. Another serious problem of using Ni-based particles is their carcinogenicity. This high risk on the surrounding puts the relative operations under special supervision resulting in extra costs as well (Adanez, 2012).

Similar to the Ni-based materials, Mn-based oxygen carriers also show relatively high capacity to convert syngas and CH_4. These materials also have the benefit of low price as well as non-toxicity. However, the effort to deal with the application of pure Mn-based oxygen carriers in continuous CLC and CLOU units is still inadequate. (Adanez, 2012).

The redox reaction for Mn materials is based on the transformation between Mn_2O_3 to MnO for CLC whereas in CLOU operation, the conversion between Mn_2O_3 and Mn_3O_4 takes place (Frick, 2016). However, it is not easy to oxidize Mn_3O_4 to Mn_2O_3 even at the low temperature conditions which are required by some kinetic limitations, not alone at high temperatures (>800 °C) where the oxidizing is thermodynamically hindered (Zafar, 2007). Furthermore, high temperatures are necessary for the complete reaction between common fuels and oxygen carriers (Kale, 2012).

Based on the previous examinations in laboratory-scale fluidized-bed reactor, the combination of Mn with other elements like Ca, Ni, Cu, Fe, Mg and Si is a good alternative to conquer the thermodynamic and kinetic constraints of oxidation and provide CLOU behavior (Jing, 2014). Taking Cu–Mn oxides as an example, they are proven to show high reactivity as well as remarkable fair reproducible behavior in redox reactions in CLOU (Arjmand, 2012). In addition, Fe–Mn oxygen carriers (Azimi, 2012), Ni-Mn oxides (Shulman, 2009) and Ca-Mn oxides (Jing, 2013) also exhibit satisfying thermodynamic properties.

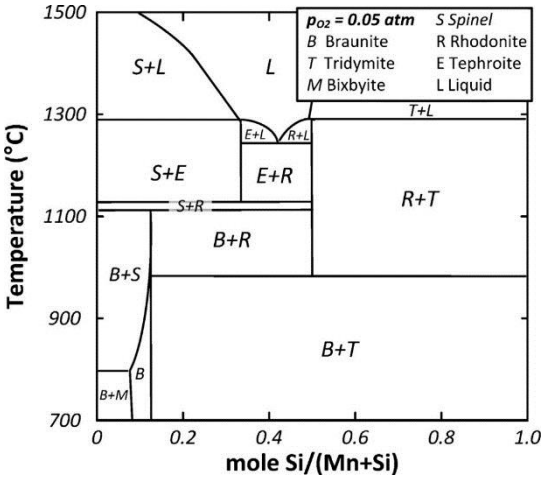


Fig. 2. Phase diagram of Mn–Si binary oxide system at O_2 partial pressure of 0.05atm (Magnus Rydén, 2014).

Another potential candidate is Mn-Si oxide which is expected to be cheap and environmental friendly. A calculated phase diagram of Mn–Si binary system under O_2 partial pressure of 0.05 atm is shown in Fig. 2. The relationship between the precise decomposition temperature and the specific composition ratios is somewhat unclear since Mn-Si combined oxides have not been studied in detail (Rydén, 2014). According to the phase diagram in Fig. 2, for Si/(Mn+Si) ranging from 0.14 to 0.50, braunite (B) Mn_7SiO_{12} reduces to rhodonite (R) $MnSiO_3$ to release oxygen when temperature grows to around 980°C, see Eq.7. In this condition, excess silicon exists as tridymite (T) SiO_2. As the temperature further increases, the mechanism to achieve oxygen release changes to conversion from rhodonite (R) $MnSiO_3$ to tephroite (E) Mn_2SiO_4 instead, see Eq.8 (Rydén, 2014).

$$\left(\frac{2}{3}\right) Mn_7SiO_{12}(B) + 4SiO_2(T) \leftrightarrow \left(\frac{14}{3}\right) MnSiO_3(R) + O_2 \qquad \text{Eq.7}$$

$$\left(\frac{2}{3}\right) Mn_7SiO_{12}(B) + \left(\frac{10}{3}\right) MnSiO_3(R) \leftrightarrow Mn_2SiO_4(E) + O_2 \qquad \text{Eq.8}$$

Thus, manganese and silica oxides become rather favorable for CLOU system taking advantage of such phase transitions accompanied by the oxygen release (Jing, 2014).

Another variable occurring in the manufacture process that may change the reactivity and stability of the oxygen carriers is calcination temperature (Frick, 2015). High calcination temperature is generally believed to cause the decline of active surface areas and porosity (HARPER, 1967). Also, furthering heating can lead to agglomeration of the oxygen carriers (Galina A. Bukhtiyarova, 2007). How the behaviors of Mn-Si oxides with support material are related to the calcination temperatures is interesting for this study.

1.4 Objective

This research focus on the assessment of reactivity of oxygen carriers towards gaseous combustibles i.e. syngas and methane. The carrier ration Si/(Mn+Si) is constant at 0.25 with different additives of Ca an Al oxides. Oxygen transport capacity and mechanical properties

are studied as well. The objective is to determine robust oxygen carriers which exhibit remarkable CLOU behavior and high combustion efficiency.

2. Experimental

2.1 Assessed oxygen carriers

As mentioned before, the thermodynamic limitations are overcome by combining silicon with Mn-based oxides. The possible oxidation temperatures of Mn-Si oxides rise to the range of 950 °C to 1050 °C. However, the poor physical strength of these oxygen carriers demands further improvement. One feasible manner is using inert compounds as support materials, which are believed to benefit both physical and chemical performance (Frick, 2015). Given the limited studies regarding Mn-Si oxygen carriers, this research aims to investigate the behavior of Mn-Si oxides with constant ratio of Mn/Si but various contents of support materials.

Two kinds of inert compounds are chosen to be the supporting material i.e. CaO and Al_2O_3. Twelve Manganese-Silicon oxygen carrier samples with a CaO content varying in the range of 2wt% and 41wt% and twelve samples with a Al_2O_3 content varying from 2wt% to 36wt% are produced by exploiting the method of spray-drying.

More detailed descriptions of manufacture procedures could be found in another study (Jing, 2013). In this study, the produced carriers were calcined in air in three calcination temperatures i.e. 1100 °C, 1150°C 1200 °C. This should not be confusing with the bed temperature described below. To satisfy the size requirements in different characterization tests, particles were sieved and categorized to 125-180μm and 180-250μm. To be more clear, fresh particles represent calcined oxygen carriers whereas particles after reactions are named as used particles. The synthesis compositions and corresponding calcination conditions are outlined in Table. 1.

Table. 1. Properties of oxygen carriers measured in this study.

Oxygen carrier	Synthesis composition[wt.%]	Calcination temperature[ºC]
Mn44SiCa41-1100 Mn44SiCa41-1150 Mn44SiCa41-1200	44% Mn_3O_4, 15% SiO_2, 41% CaO	1100 1150 1200
Mn59SiCa21-1100 Mn59SiCa21-1150 Mn59SiCa21-1200	59% Mn_3O_4, 20% SiO_2, 21% CaO	1100 1150 1200
Mn71SiCa5-1100 Mn71SiCa5-1150 Mn71SiCa5-1200	71% Mn_3O_4, 24% SiO_2, 5% CaO	1100 1150 1200
Mn74SiCa2-1100 Mn74SiCa2-1150 Mn74SiCa2-1200	74% Mn_3O_4, 24% SiO_2, 2% CaO	1100 1150 1200
Mn48SiAl36-1100 Mn48SiAl36-1150 Mn48SiAl36-1200	48% Mn_3O_4, 16% SiO_2, 36% Al_2O_3	1100 1150 1200
Mn62SiAl17-1100 Mn62SiAl17-1150	62% Mn_3O_4, 21% SiO_2, 17% Al_2O_3	1100 1150
Mn69SiAl7-1150	69% Mn_3O_4, 24% SiO_2, 7% Al_2O_3	1150
Mn72SiAl4-1100 Mn72SiAl4-1150 Mn72SiAl4-1200	72% Mn_3O_4, 24%SiO_2, 4% Al_2O_3	1100 1150 1200
Mn74SiAl2-1100 Mn74SiAl2-1150 Mn74SiAl2-1200	74% Mn_3O_4, 24% SiO_2, 2% Al_2O_3	1100 1150 1200

2.2 Experimental method and setup for reactivity test

In order to identify the gas-phase oxygen release ability as well as the conversion capability towards fuel gas i.e. methane and syngas (50 vol.% H_2 in CO) of the obtained oxygen carriers, a lab-scale fluidized bed reactor of quartz is utilized. The reactor with a total length of 870 mm and 22-mm diameter in the reaction zone is heated in an electrically controlled furnace. A sample of 15 g particles (125–180μm) is supported by a porous quartz plate which is 370 mm from the bottom of the reactor.

Error! Reference source not found. gives an overview of the experimental setup. The gas is fed into the system from the bottom. Several mass flow regulators are applied to control the inflowing gas flows. When the system is required to provide oxidizing, inert or reducing conditions, embedded electric valves are switched automatically in accordance with a pre-defined progression, as shown in Table. 2 (Jing, 2014). Thermocouples are placed 5 mm underneath the plate to monitor the feeding gas temperature and in the actual bed (25 mm above the plate) for the temperature measurement of the fluidized bed. To verify the steady fluidization of the bed materials, the pressure drop over the fluidized bed, which is expected to be highly fluctuating, is assessed constantly (Mohammad Pour, 2013). The condensation of off-gas and remove of the condensed water are followed by the quantification of the volume fractions of the effluent in a Rosemount NGA-2000 analyzer (Jerndal, 2011). Thus, all the evaluations are given on dry basis.

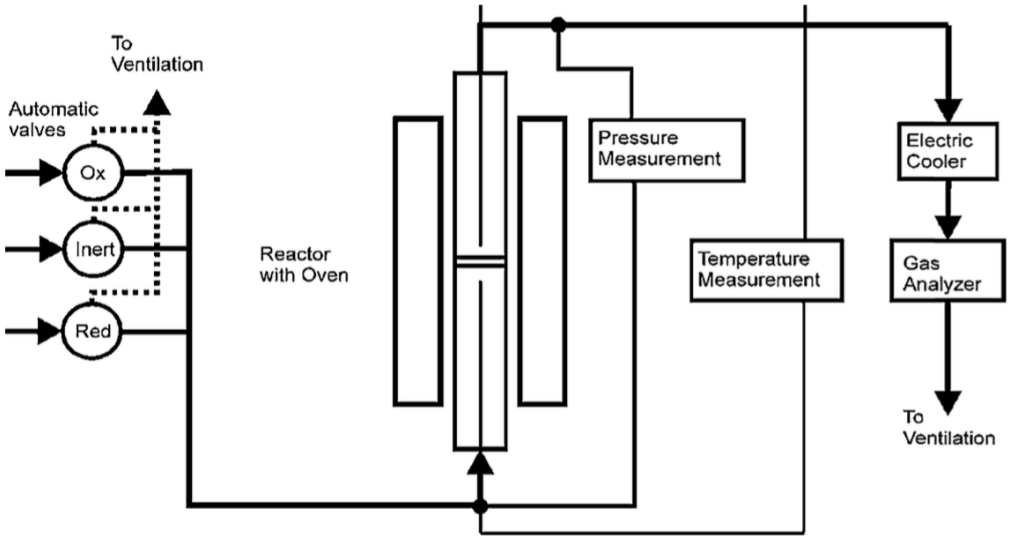


Fig. 3. Scheme of the experimental setup.

Table. 2. Experimental procedure used to investigate oxygen release and gas conversion.

Gas composition	Bed temperature[°C]	No. of cycles	Duration inert period[s]	Duration N_2-purge[s]	Duration reduction period[s]
50 vol.% CO in H_2	950	2	-	60	80
100 vol.% CH_4	850	2	-	60	20
100 vol.% N_2	850	2	360	-	-
100 vol.% CH_4	950	2	-	60	20
100 vol.% N_2	950	2	360	-	-
100 vol.% CH_4	1050	2	-	60	20
100 vol.% N_2	1050	2	360	-	-
100 vol.% CH_4	950	2	-	60	20
100 vol.% N_2	950	2	360	-	-

Sufficient fluidization of the bed materials is vital to guarantee stable operations. Hence, it is necessary to feed the gases with much higher velocity than the minimum gas flowrate required for fluidizing. In this study, feeding gas velocities of 900 ml/min, 450 ml/min and 600 ml/min are applied in the oxidizing, reducing periods and inert period respectively, the detailed explanation can be found in other studies (Frick, 2016).

The assessed oxides in the fluidized bed are exposed in the oxidizing atmosphere until the bed temperature reaches the set temperature i.e. 850 °C, 950°C, 1050 °C. These operating temperatures are chosen since oxygen carriers cannot convert combustibles sufficiently with too low temperatures whereas the particles tend to agglomerate in too high temperatures. This should not be confusing with the calcination temperature mentioned above. Moreover, the particles are oxidized by 5 vol.% of oxygen in nitrogen (Sundqvist, 2015). On one side, it is known that the oxidizing is a highly exothermic process. Thus, this low oxygen concentration can prevent the immediate temperature boost (Jerndal, 2011). On the other side, high excess air caused by low oxygen concentration will lead to low thermal efficiency of the process and higher expenditure. Thus, the oxygen concentration in the exit gas stream from a large scale air reactor is assumed to be 5 vol.% (Rydén, 2014).

When determining the reactivity of oxygen carriers towards the gaseous fuels, the oxidized particles are placed in inert and reducing atmospheres in sequence. In the reducing conditions, two kinds of gaseous combustibles are studied (syngas and methane), as mentioned before. Since four times more O_2 per mole of gas is in demand when combusting gaseous methane than syngas, fueling syngas costs four times longer time (Frick, 2016). Because the fuel gases may react with remaining oxygen from the previous step, nitrogen is used to flush the reactor for 60 s between each oxidizing and reducing period to avoid assessment deviations (Sundqvist, 2015). One cycle indicates a progression of the reducing period followed by the oxidizing period. Operating at least two times of all the cycles is vital to assure the stable behavior of the operation and reliable assessment. Before undergoing the following reducing conditions, the depleted oxygen carriers are regenerated until the measured O_2 content rises back to 5 vol.% again and keeps steady for a while (Frick, 2016).

In terms of measuring the oxygen release ability of the particles, the duration time in nitrogen is 360 s, which is long enough to get a comprehensive evaluation. The computer analyzes the exhaust gases and records the oxygen volume fraction. Only the average oxygen content value in the last 300 s is needed for the further assessment since the oxygen might be the remaining oxygen from the preceding oxidizing periods rather than the oxygen released by the particles in the first 60 s. The oxidizing rate is not included in this study since this step is very fast indicating that the full consumption of all feeding-in oxygen can be obtained at the beginning of this period (Jing, 2014).

Fig. 4 to Fig. 6 show the effluent concentrations as a function of time in inert period, fuel period towards syngas and gaseous methane individually and the testing sample is Mn71SiCa5-1150. In the reducing period of syngas, the converting speed is dramatically fast. The syngas, which is just fed into the reactor, is consumed immediately. By contrast, the conversion ability towards methane is weaker. Only the oxygen content occurs and varies in the inert period. The oxygen concentration decreases to nearly zero when the inert period starts due to the high flux of nitrogen. When the inert period finishes and oxidation starts, the oxygen content increases quickly back to 5 vol.%. More details will be described later in the article. In addition, in case that the harsh conditions exert damage on the particles, all kinds of assessments have to proceed once more time in 950 °C after 1050 °C.

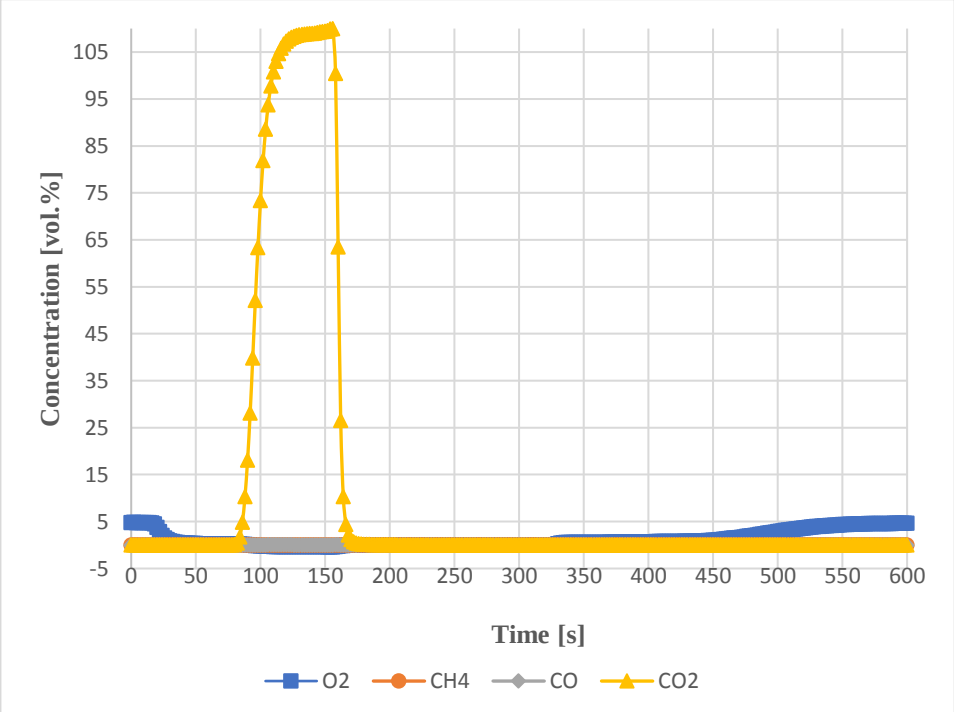


Fig. 4. Off-gas concentration profile of the second syngas cycle at 950 ºC using Mn71SiCa5-1150 oxygen carrier.

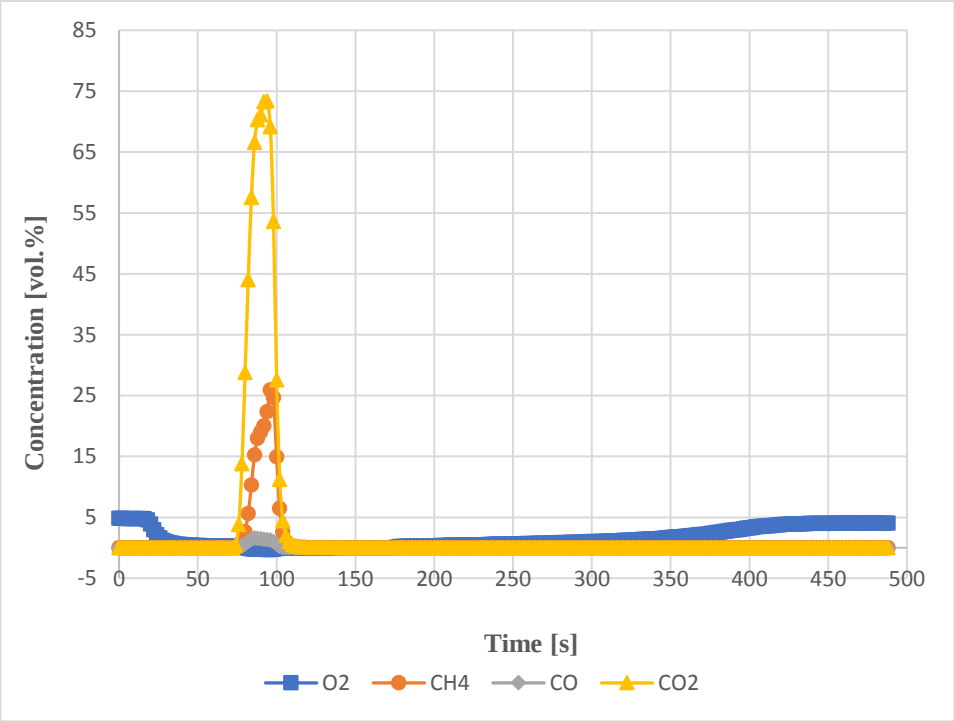


Fig. 5. Off-gas concentration profile of the second methane cycle at 950 ºC using Mn71SiCa5-1150 oxygen carrier.

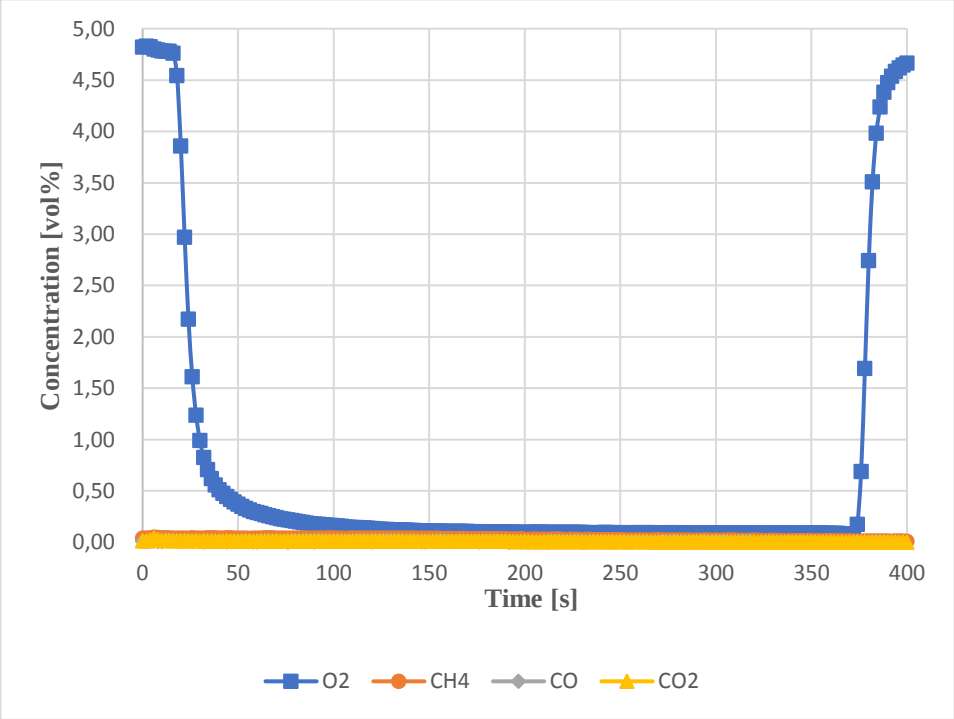


Fig. 6. Off-gas concentration profile of the second inert cycle at 950 ºC using Mn71SiCa5-1150 oxygen carrier.

2.3 Data evaluation

The combustion performance of the oxygen carriers is quantified by the amount of formed carbon dioxide γ_{CO2}, which is calculated using Eq.9. The denominator indicates the total gas concentrations of carbon species in the off-gas streams (Källén, 2014). The volume fraction of component i in the exhaust gas flow is represented by y_i.

$$\gamma_{CO_2} = {y_{CO_2}}/{(y_{CO} + y_{CO_2} + y_{CH_4})} \quad \text{Eq.9}$$

Furthermore, oxygen carrier conversion ω is defined as the current particle mass $m_{current}$ divided by the mass of their fully oxidized state $m_{oxdized}$, see Eq.10. $m_{oxdized}$ is simplified to be 15 g, which is the mass of the fresh oxygen carriers, the possible variation of mass caused by the high temperatures is neglected (Jing, 2014).

$$\omega = {m_{current}}/{m_{oxidized}} \ [-] \quad \text{Eq.10}$$

However, it is not possible to weigh the mass of oxygen carriers directly during the operation. One feasible solution is calculating the current mass of the particles as a function of time from the off-gas content through O_2 mass balance in the fluidized bed (Rydén, 2014). Thus, calculations of creativity of oxygen carriers with gas-phase methane and syngas are expressed by Eq.11 and Eq.12 respectively. Mo_2 denotes the O_2 molar mass while n is the off-gases molar flowrate. One thing has to be mentioned is that the measurement of the volume fraction of hydrogen is not included in this study. H_2 reacts much faster than CO with O_2 (Jerndal, 2011). Furthermore, the content of CO remains at a quite low level in all cases, see Fig. 4 to Fig. 6. Thus, it is reasonable to assume the full conversion of H_2.

$$\omega_i = \omega_{i-1} - \int_{i-1}^{i} \frac{nM_{O_2}(4y_{CO_2}+3y_{CO}+2y_{O_2}-y_{H_2})}{m_{oxidized}} dT \quad \text{Eq.11}$$

$$\omega_i = \omega_{i-1} - \int_{i-1}^{i} \frac{nM_{O_2}(2y_{CO_2}+y_{CO}+y_{O_2}-y_{H_2})}{m_{oxidized}} dT \quad \text{Eq.12}$$

Characteristic number $\bar{\gamma}_{CO_2}$ (the average valued of produced carbon dioxide) calculated in the range of 0.99-1.00 enables the comparison between the fuel conversion abilities of oxygen carrier particles in various operating temperatures.

2.4 Characterization of materials

In industry-scale CLC and CLOU operation, mechanical durability is one of the basic standards for oxygen-carriers to be recognized as practical. The attrition and fracture of the materials should be as low as possible. The force to create fragmentation of the particles can be characterized by measuring the crushing strength using a Shimpo FGN-5 crushing strength apparatus. To minimize the assessment error, 30 particles (180-250μm) are crushed to obtain their average value for each sample (Jerndal, 2011).

In order to determine the attrition resistance of different samples, a laboratory-scale attrition rig is applied based on the jet cup method under ambient condition and roughly atmospheric pressure (Fig. 7). More description of the apparatus can be found in the previous study (Rydén, 2014).

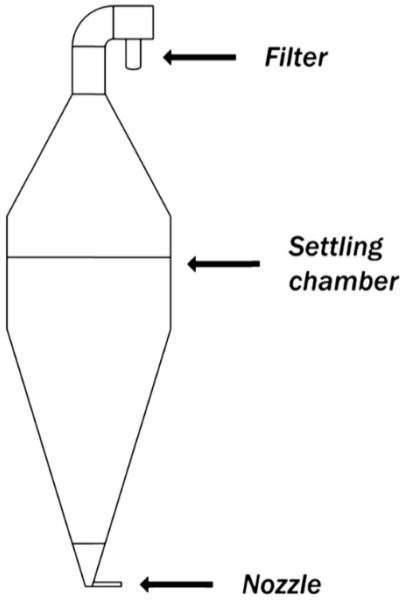


Fig. 7. Schematic representation of lab scale attrition rig (Rydén, 2014).

5 grams used particles are placed inside in each attrition measurement test. These particles are then exposed to a high velocity gas jet (around 100 m/s) and may be subjected to abrasion through collision with each other and with the reactor walls as well and result in the fragmentation of the weak particles (Mohammad Pour, 2013).

A filter is located at the top of the separator to collect the fine particles. The filter is dismantled to measure the weight every 10 minutes. The whole duration time of the test is 60 minutes (Rydén, 2014). The attrition index A can be determined based on the data recorded in the last 30 minutes according to Eq.13.

$$A = \frac{m_{t=60min} - m_{t=30min}}{m_{initial}} \times \frac{60}{30} \times 100[wt.\%/h] \qquad \text{Eq.13}$$

In this equation, $m_{initial}$ denotes the initial particle mass while m_t represents the mass of the fines collected by the filter at time t (Frick, 2016).

To analyze the phase composition of the metal oxides, X-ray diffractometry method is used (Frick, 2016). Furthermore, to study the reduction mechanism, both the X-ray spectra of the samples oxidized in 5 vol.% O_2 and fully reduced are compared (Mohammad Pour, 2013).

3. Results

3.1 CLOU properties (Oxygen release)

In order to make a clear comparison on the oxygen release capability of different oxide particles, the corresponding calculated average O_2 concentrations in the inert conditions at three bed temperatures are summarized in Fig. 8 and Fig. 9. As mentioned before, to check whether the oxygen carrier particles suffer deterioration in the highest bed temperature (1050 °C), the tests are operated at 950 °C again. Thus, the data obtained from the second operation in 950 °C are listed to compare with data of the first time as well.

As shown in Fig. 8, Mn-Si oxides supported by CaO with higher support materials' content always show significantly low oxygen release, without regard for the calcination temperature. In contrast, for the oxygen carrier particles with lower CaO content (below 5 wt.% CaO), calcination temperature seems to play an important role in their performance.

Regarding the Mn-Si oxygen carriers using Al_2O_3 as supporting materials, data are depicted in Fig. 9. It becomes hard to get clear rule since only the particle Mn69SiAl7-1150, Mn72SiAl4-1100 and Mn72SiAl4-1150 perform remarkably. Both production temperature and compositions ratios have big effect on the oxygen carrier performance.

It is clear that higher temperatures in the fluidized bed are always accompanied with higher O_2 content in the effluent, regardless of composition ratios and calcination temperatures. This is also in line with the phase transitions show in Fig. 2. The oxygen release ability is quite low with supporting materials higher than 21 wt.%, no matter CaO or Al_2O_3.

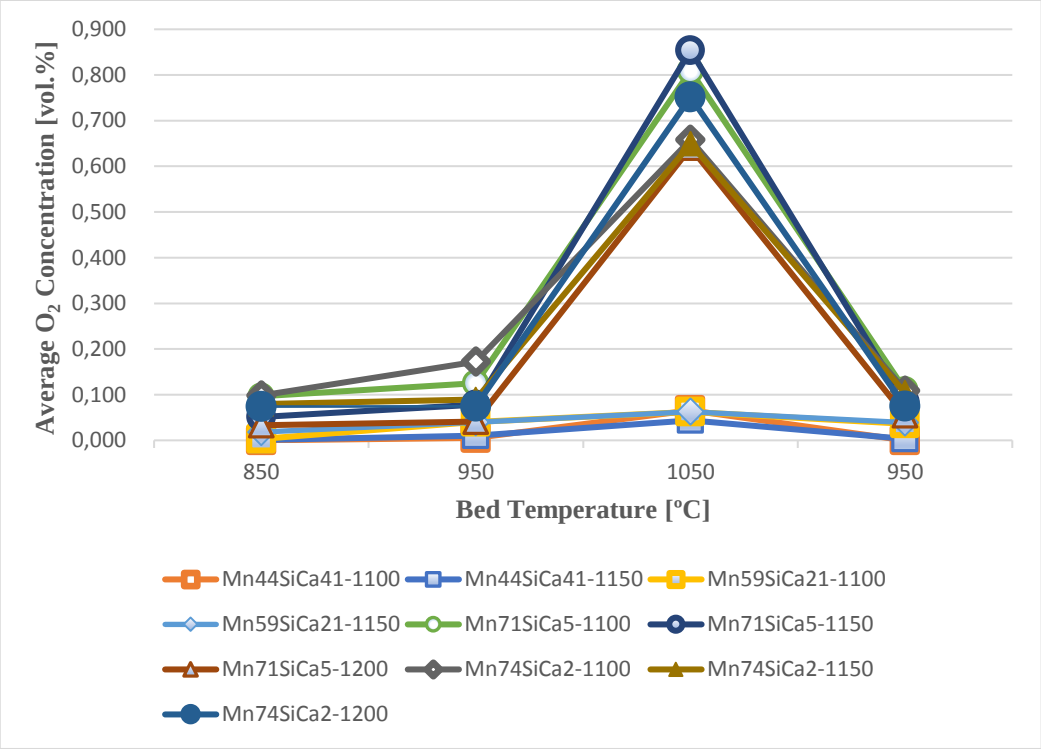


Fig. 8. Average O_2 concentration during inert period for Mn-Si oxygen carriers supported by CaO.

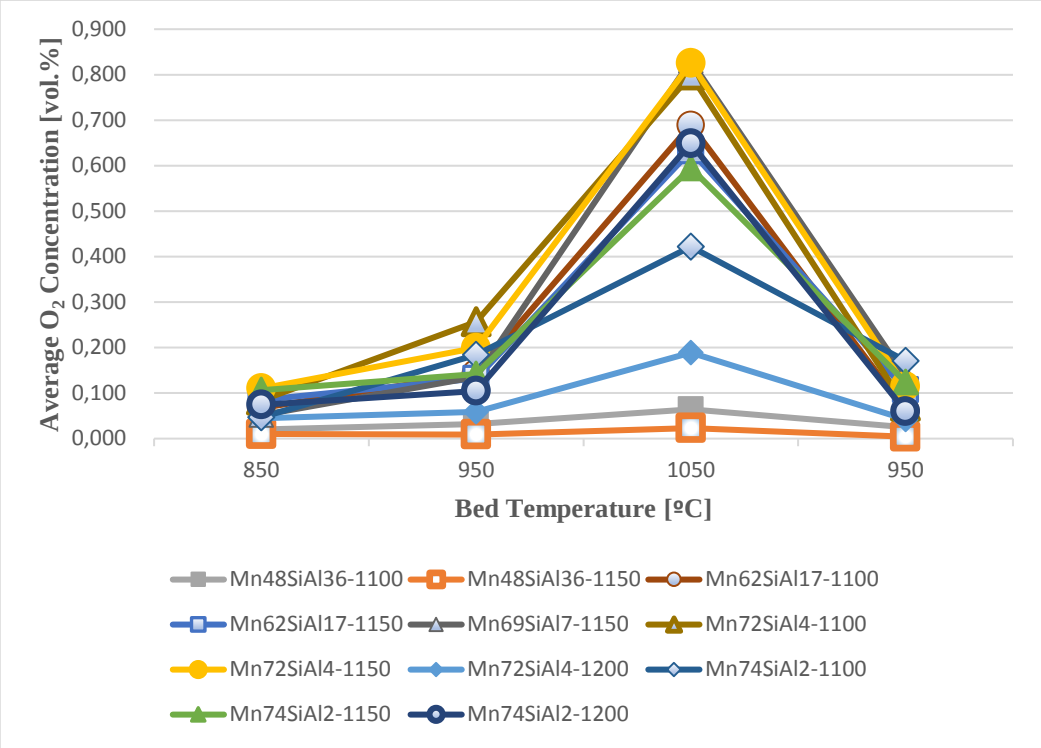


Fig. 9. Average O_2 concentration during inert period for Mn-Si oxygen carriers supported by Al_2O_3.

To further figure out the influence of the calcination temperature during production on the final oxygen release behavior, Mn71SiCa5 and Mn72SiAl4, which have the best performance in the previous assessments, are picked out. It can be seen in from Fig. 10, the difference of the results between Mn-Si based materials supported by CaO with the same compositions obtained from the manufacture temperature 1100 °C and 1150 °C is marginal. Yet the material with the identical content calcined in 1200 °C exhibits much lower oxygen release. The effect caused by the calcination temperature becomes even more pronounced in Mn-Si oxides with Al_2O_3 as support materials when looking at the values in Fig. 11. It could also be concluded that the effect of the production temperature is more obvious at higher bed temperature (1200 °C). The explanation for this phenomenon could be that too high calcination temperature damages the structure of the particles and high bed temperatures even worsen these existing deteriorations.

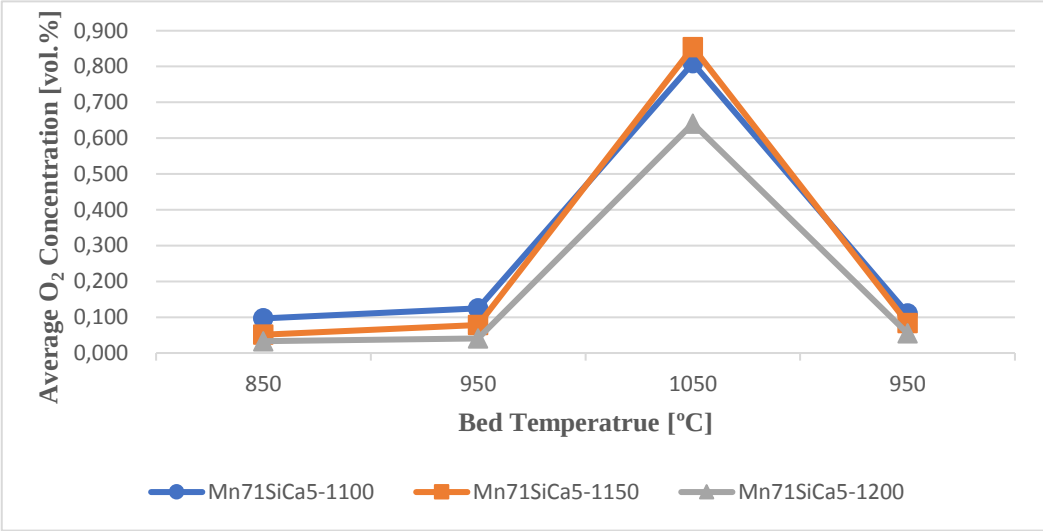


Fig. 10. Average O_2 concentration during inert period for Mn71SiCa5 calcined in three temperatures.

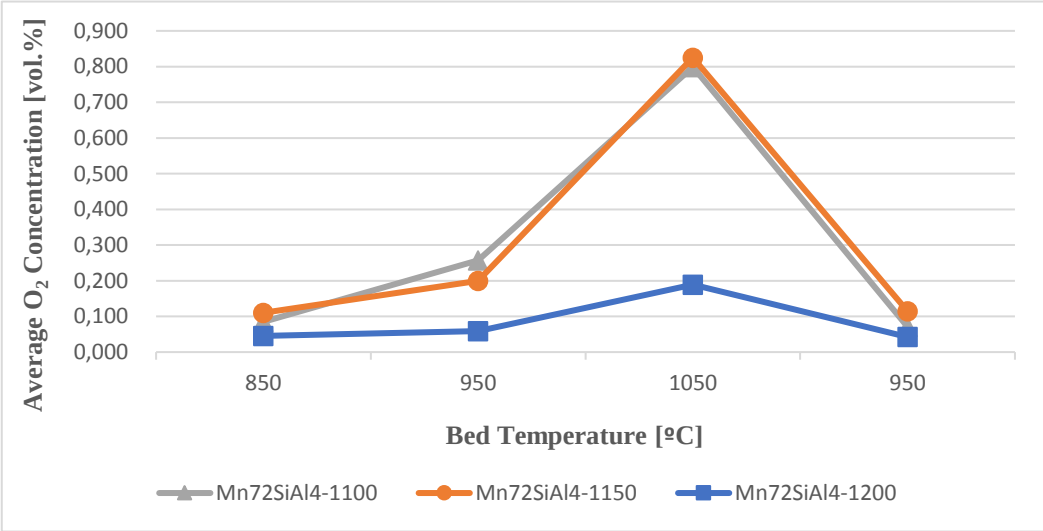


Fig. 11. Average O_2 concentration during inert period for Mn72SiAl4 calcined in three temperatures.

3.2 Reactivity test

3.2.1 Fuel gas conversion capacity of Mn-Si oxides supported on CaO

With respect to the assessment of the reactivity of the oxygen carriers with fuel gas, the inlet gases conversions of the Mn-Si particles with CaO support material which are expressed by carbon dioxide yield are depicted in Fig. 12 and Fig. 13. As seen all particles convert CO very well and no distinction between the particles can be made. Since the combustion speed of H_2 is much faster than CO, full conversion of H_2 can be assumed.

It is apparent that particles show noteworthy stable conversions towards syngas in the bed temperature 950 °C in all cases (Fig. 12). However, the experiments are designed to investigate differences and full conversion of CH_4 is not expected, see Fig. 13. The Mn-Si based oxygen carriers with 5 wt.% CaO produced at a calcination temperature of 1100 °C and 1150 °C show steady high reactivity towards CH_4. The trend is similar for the particles with 2 wt.% CaO content. It could be suggested that both lower calcination temperatures and lower CaO content contribute to the good ability of fuel conversion with CH_4.

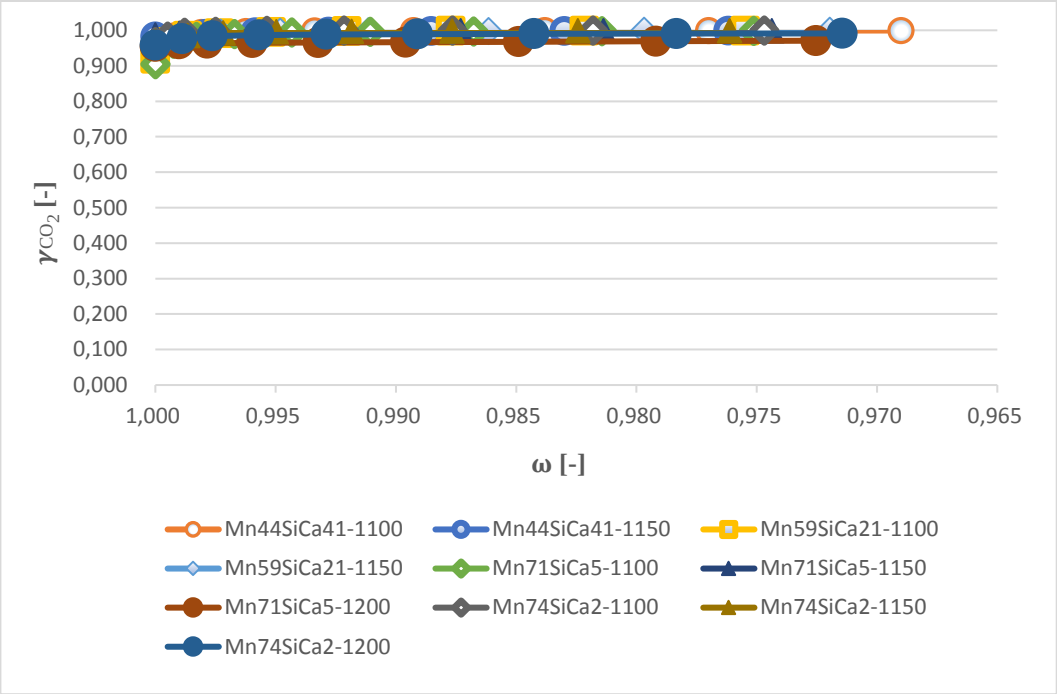


Fig. 12. CO_2 yield as a function of oxygen carrier conversion of syngas at 950 °C for Mn-Si oxygen carriers supported by CaO.

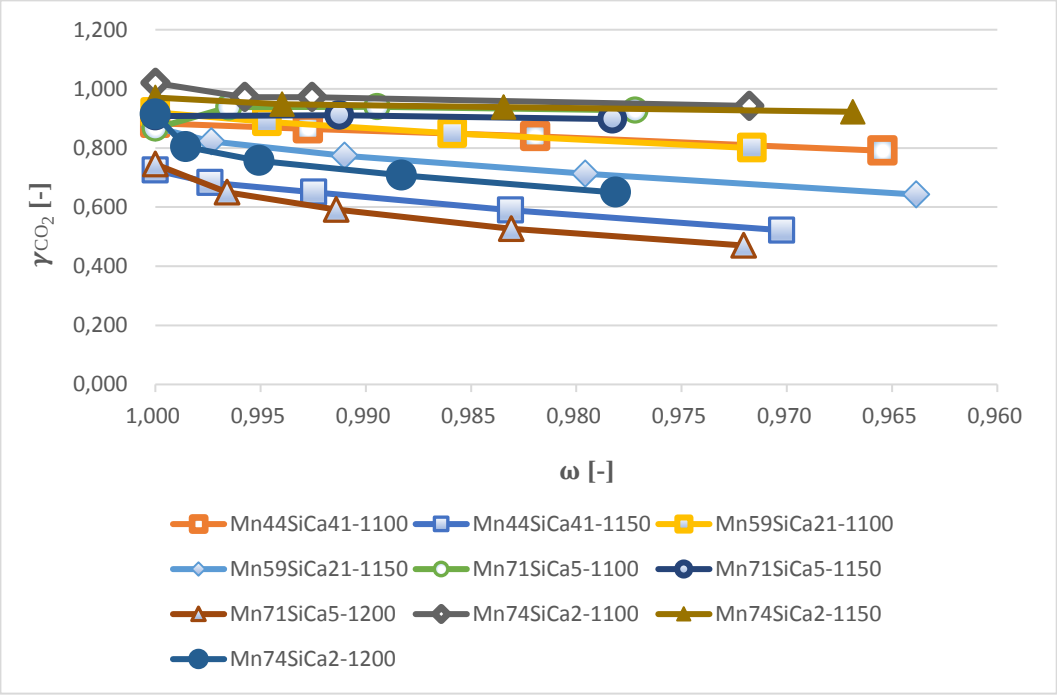


Fig. 13. CO_2 yield as a function of oxygen carrier conversion of methane at 950 °C for Mn-Si oxygen carriers supported by CaO.

In addition to the composition ratios and manufacture temperature, the relationship between gas-phase methane conversion capability and the bed temperatures is also worth considering. Fig. 14 illustrates the average carbon dioxide yield as a function of the bed temperature. It is clear that the performance of the oxygen carriers benefits from the hotter fluidized bed

conditions in all cases. The average carbon dioxide yield reaches above 0.8 in bed temperature of 1050 °C with no exception.

Moreover, almost all the oxygen carriers maintain their reactivity at 950 °C after the reducing period at bed temperature of 1050 °C except Mn71SiCa5 and Mn74SiCa2 pretreated at 1200 °C. It is likely that their structures alter as a consequence of high calcination temperature along with tough operating conditions.

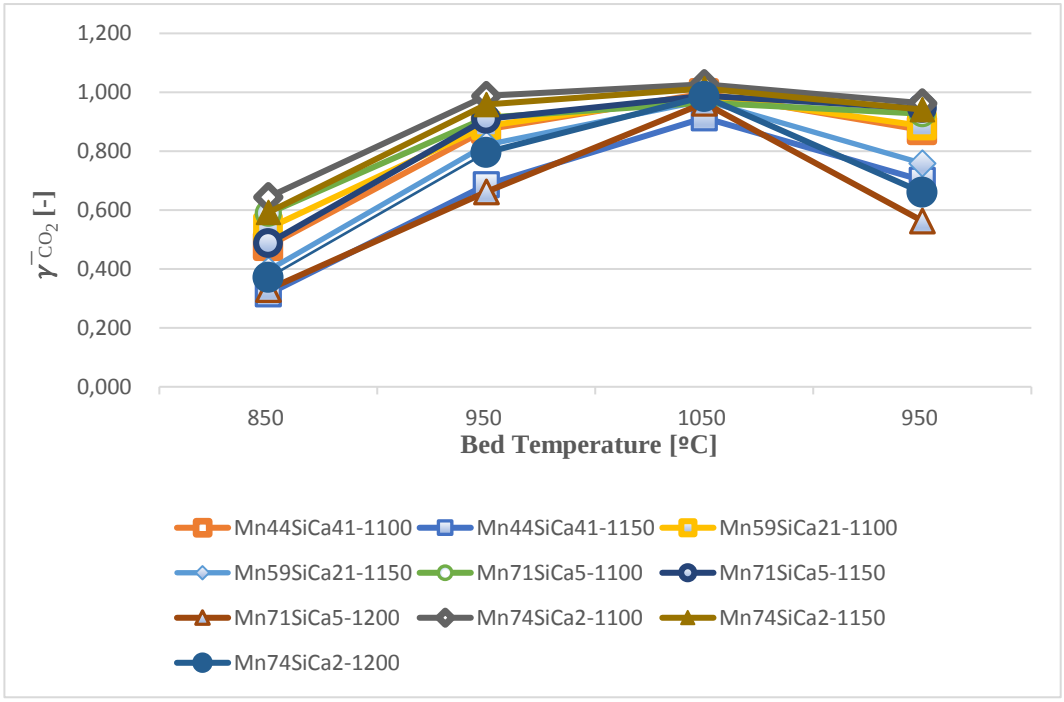


Fig. 14. Average CO_2 yield as a function of the bed temperature of methane at 950 °C for Mn-Si oxygen carriers supported by CaO.

3.2.2 Fuel gas conversion capacity of Mn-Si oxides supported on Al_2O_3

With respect to the Mn-Si oxygen carriers supported by Al_2O_3, the support materials' content shows significant effect on the fuel conversion towards syngas. As shown in Fig. 15, the ability of Mn48SiAl36-1200 and Mn48SiAl36-1100 to convert syngas exhibit a constant drop. All other ten oxygen carriers perform well and steadily. High Al_2O_3 content tends to negatively affect fuel conversion, while the influence of calcination temperatures on the materials is kind of ambiguous. A similar effect of composition ratio can also be seen from the performance of methane conversion in Fig. 16. Additionally, the adverse impact of high manufacture temperature on the oxygen carriers becomes obvious as well. More analysis will be given later in the report. Only the particles Mn72SiAl4-1100, Mn74SiAl2-1100 and Mn74SiAl2-1150 exhibit a noteworthy stable fuel conversion capability constantly (above 0.8).

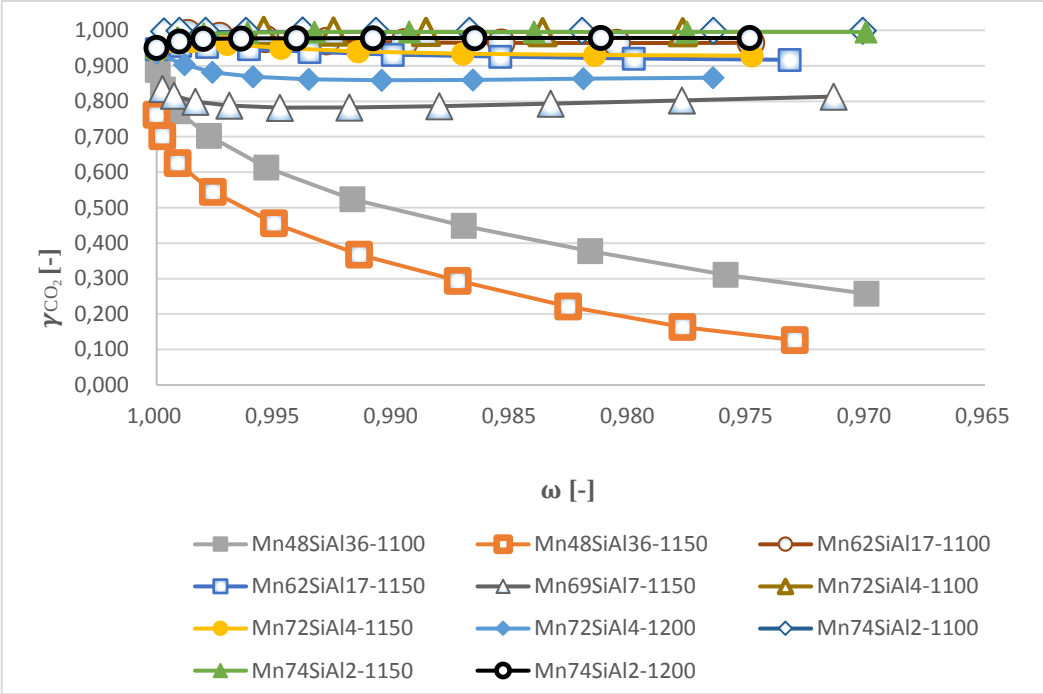


Fig. 15. CO_2 yield as a function of oxygen carrier conversion of syngas at 950 °C for Mn-Si oxygen carriers supported by Al_2O_3.

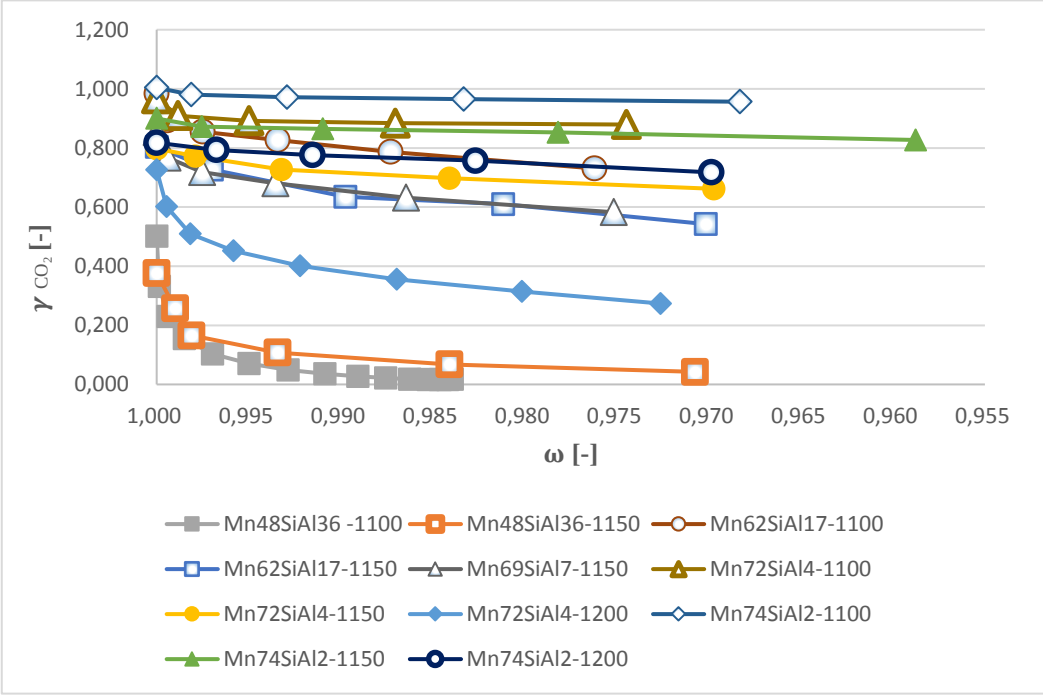


Fig. 16. CO_2 yield as a function of oxygen carrier conversion of methane at 950 °C for Mn-Si oxygen carriers supported by Al_2O_3.

Unlike the stable performance of the Mn-Si oxygen carriers supported by CaO, significant deviation can be observed for the fuel conversion capability of some particles supported by Al_2O_3 after undergoing strong reducing conditions, especially for Mn72SiAl4-1200 and Mn74SiAl2-1200 (Fig. 17). Thus, the same hypothesis can be made for Mn-Si oxides with

Al_2O_3 support material, the structure of the materials obtained from strong calcination conditions tends to be more fragile when being applied in the high bed temperatures.

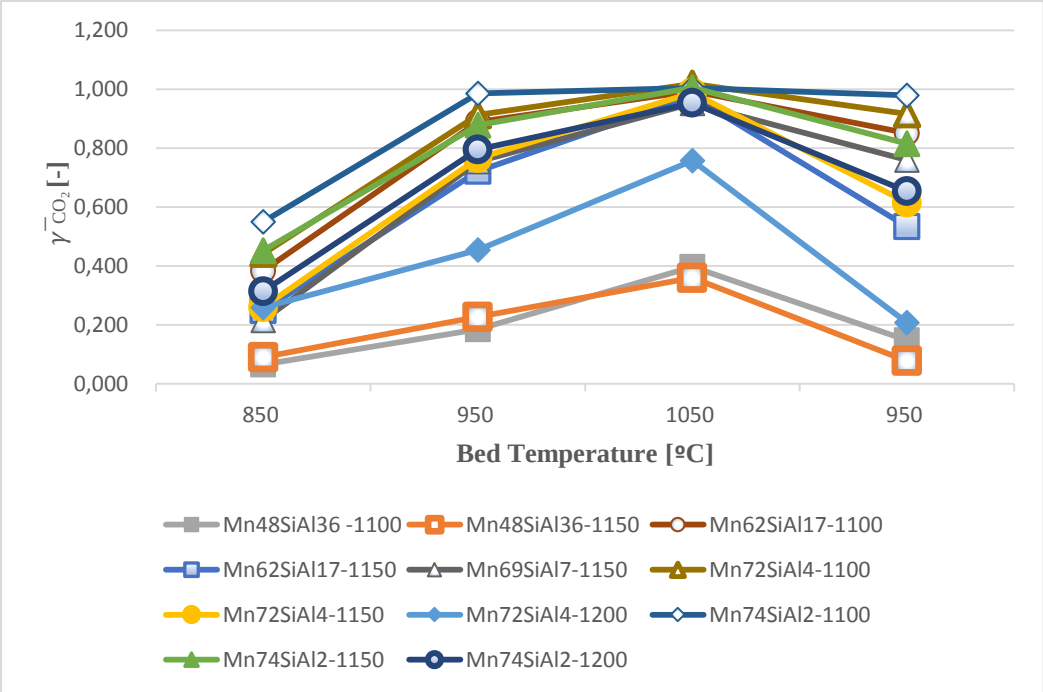


Fig. 17. Average CO_2 yield as a function of the bed temperature of methane at 950 °C for Mn-Si oxygen carriers supported by Al_2O_3.

As analyzed in the part of oxygen release capacity in Fig. 10 and Fig. 11, calcination conditions have a consequence to the behavior of the oxygen carrier particles. Thus, whether the calcination temperature has a similar effect on fuel conversion is also interesting. The oxygen carriers with the identical compositions as assessed previously i.e. Mn71SiCa5 and Mn72SiAl4 are chosen to be evaluated again. It can be found from Fig. 18 and Fig. 19, the influence seen from the high production temperatures on the fuel gas conversion is even more distinct than that on the oxygen release. The conversion ability of Mn-Si particles experiences continual decrees regardless of the supporting materials, which also proves that too high manufacture temperature is the main limiting factor for good reactivity.

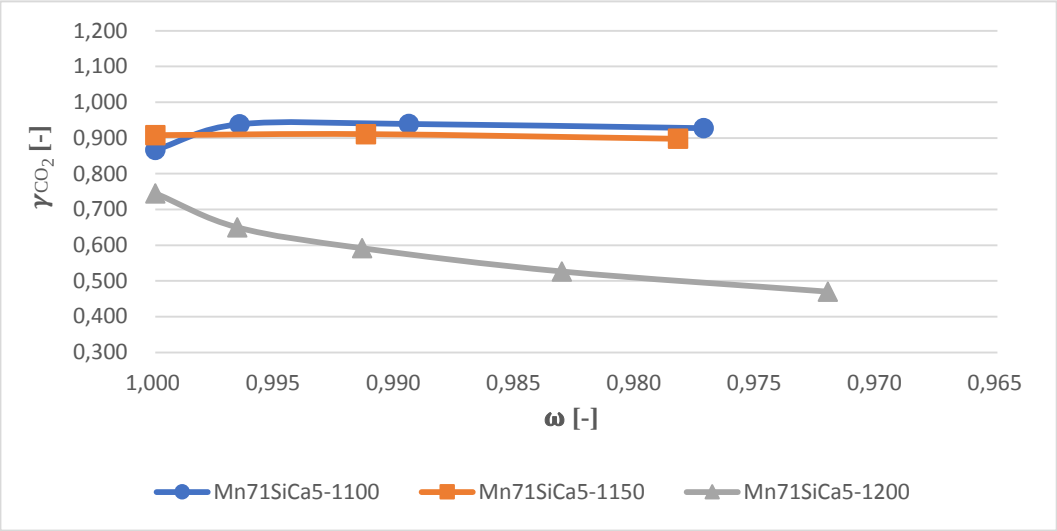


Fig. 18. CO_2 yield as a function of oxygen carrier conversion of methane for Mn71SiCa5 calcined in three temperatures.

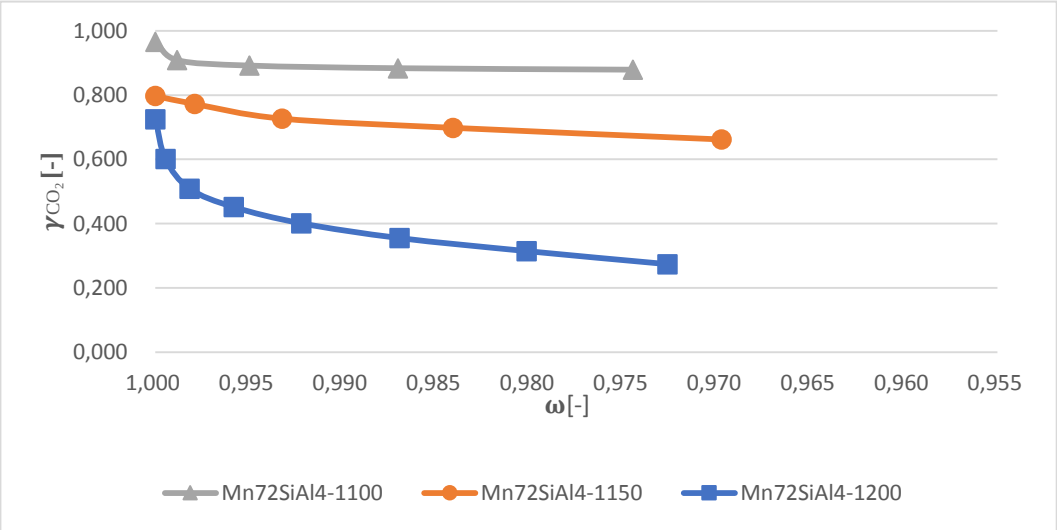


Fig. 19. CO_2 yield as a function of oxygen carrier conversion of methane for Mn72SiAl4 calcined in three temperatures.

3.3 Mechanical properties

In addition to the high fuel conversion and good fluidization behavior, neither considerable abrasion nor serious fragmentation of oxygen carrier particles is allowed for continuous fluidized-bed operation. Studies on the crushing strength of fresh oxygen carriers and their corresponding attrition rate after operation are done to assess the mechanical characteristics of the materials. Table. 3 and Table. 4 list all the corresponding assessment results.

Regarding the Mn-Si oxygen carriers supported by CaO, their crushing strengths are almost independent on the calcination temperature, see Table. 3. Meanwhile, the oxygen carriers calcined from 1150 °C show highest attrition index in three manufacture temperatures. No obvious correlation between production conditions and mechanically durability could be found. This suggests that their mechanical characteristics may change remarkably due to the previous experiment steps.

In contrast, the influence of calcination temperature becomes clearer for the particles with Al_2O_3 as support. It can be seen from Table. 4, higher crushing strength due to the higher calcination conditions can be connected to mechanical properties. The same conclusion can be achieved from their corresponding decreasing attrition index. A similar trend can only be recognized in Mn71SiCa5 and Mn74SiCa2 with CaO supporting materials from certain calcination temperatures. That is to say, these two kinds of materials exhibit higher crushing strength but lower attrition index when the calcination temperature changes from 1150 °C to 1200 °C.

Table. 3. Crushing strength of fresh particles and attrition index of used particles for Mn-Si oxygen carriers supported by CaO.

Oxygen carrier	Crushing strength [N]	Attrition index [wt.%/h]
Mn44SiCa41-1100	1.0	7.1
Mn44SiCa41-1150	1.5	51.9
Mn59SiCa21-1100	2.0	4.4
Mn59SiCa21-1150	1.6	18.6
Mn71SiCa5-1100	1.6	2.4
Mn71SiCa5-1150	2.1	25.1
Mn71SiCa5-1200	1.6	0.5
Mn74SiCa2-1100	1.6	23.5
Mn74SiCa2-1150	2.1	117.1
Mn74SiCa2-1200	1.6	1.1

Table. 4. Crushing strength of fresh particles and attrition index of used particles for Mn-Si oxygen carriers supported by Al_2O_3.

Oxygen carrier	Crushing strength [N]	Attrition index [wt.%/h]
Mn48SiAl36-1100	0.6	1.2
Mn48SiAl36-1150	1.6	0.4
Mn62SiAl17-1100	0.6	6.0
Mn62SiAl17-1150	1.5	3.8
Mn69SiAl7-1150	0.8	0.4
Mn72SiAl4-1100	0.6	2.9
Mn72SiAl4-1150	1.1	5.4
Mn72SiAl4-1200	2.4	0.3
Mn74SiAl2-1100	0.6	5.1
Mn74SiAl2-1150	1.1	3.1
Mn74SiAl2-1200	1.3	0.6

Oxygen carriers with high gas conversion capacity together with limited physical changes are preferred during redox reactions. From Table. 3 and Table. 4, there is no big variation of the crushing strengths of all the oxygen carriers. Thus, to figure out whether the particles in this study deserve further investigation, the average carbon dioxide production at bed temperature of 950 °C is plotted against the attrition index, see Fig. 20 and Fig. 21. With respect to the Mn-Si oxides with CaO supporting material, Mn74SiCa2-1150 and Mn44SiCa41-1150 are not included in the comparison due to their extremely small resistance to attrition (Fig. 20). Oxygen carriers Mn71SiCa5-1150, Mn59SiCa21-1100, Mn71SiCa5-1100 and Mn74SiCa2-

1100 can be seen as potential candidates with relatively low attrition index indicating rather good mechanical properties.

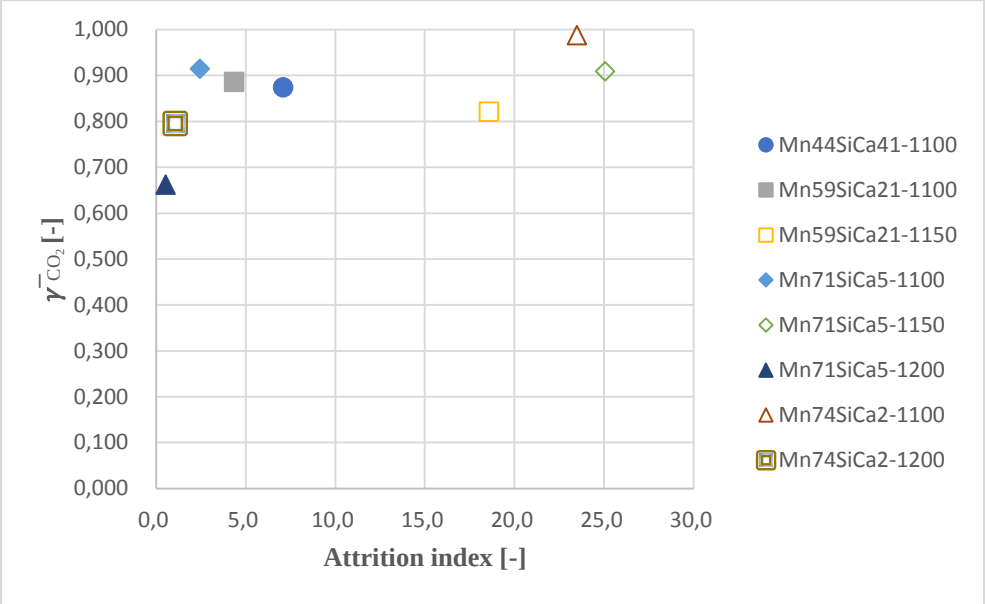


Fig. 20. Average CO_2 yield for methane conversion at 950 °C as a function of attrition index for Mn-Si oxygen carriers supported by CaO.

The same evaluation method as for the Mn-Si-based particles supported by CaO is applied for the particles with Al_2O_3 as supporting material. The oxygen carriers Mn62SiAl17-1100, Mn72SiAl4-1100, Mn74SiAl2-1100, Mn74SiAl2-1200 and Mn74SiAl2-1150 are most interesting particles since their gas conversions are fairly high, see Fig. 21. When considering the attrition rate, Mn74SiAl2-1150 and Mn72SiAl4-1100 are a little bit deficient in mechanical property with somewhat high attrition index, but can still be regarded as potential candidates. However, Mn62SiAl17-1100 and Mn74SiAl2-1100 should be removed from the candidate list due to their relatively low resistance to attrition.

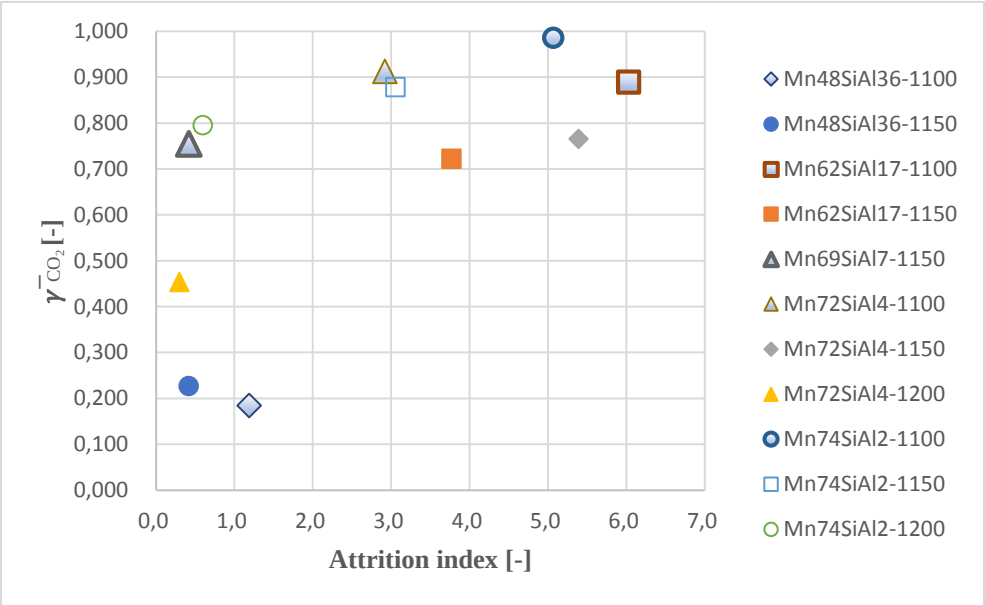


Fig. 21. Average CO_2 yield for methane conversion at 950 °C as a function of attrition index for Mn-Si oxygen carriers supported by Al_2O_3.

3.4 X-ray diffraction results

The X-ray diffraction is applied to investigate the crystalline phase of the fresh and used oxygen carrier particles. The evaluation results are shown in Table. 5 and Table. 6. Based on the corresponding compounds in the initial and final state, it is possible to check whether regeneration of the oxygen carriers after reducing conditions is successful or not.

The main manganese-containing phases detected for almost all the Mn-Si-based oxygen carriers with support materials' content of 4 wt% or less are braunite Mn_7SiO_{12} and rhodonite $MnSiO_3$. While for the particles with support materials' content above 4 wt% and below 36 wt%, Mn_7SiO_{12} or $MnSiO_3$ is predominant relating to the content of support materials, except the oxygen carrier Mn59SiCa21-1200. It can be concluded that higher calcination temperature along with less support materials' content contribute to the formation of manganese silicates.

As known from the discussion in section 1.3, the necessary temperatures for CLOU hinder the bixbyite Mn_2O_3 to contribute to the CLOU oxygen release performance and react directly with the fuel gases (CH_4/syngas). Hence, manganese silicates are supposed to be the actual active phases in the reactions. However, to guarantee that the manganese silicates facilitate the reaction significantly, too large amount of support materials is problematic. As shown in Table. 5, the amount of braunite Mn_7SiO_{12} and rhodonite $MnSiO_3$ in the particles increases with less support materials' content, and their reactivity behaviors are promoted correspondingly, as confirmed by the previous assessments related to fuel gas conversion and CLOU oxygen release. Theoretically, the best oxygen carrier behavior should occur with the most production of braunite Mn_7SiO_{12}. Calculating using the reaction Eq.7, the supposed SiO_2 content should be 45wt% according to stoichiometric calculation. However, in reality, particles with around 24wt% content are preferred due to the better reactivity properties.

With respect to the particles with support materials' content more than 36wt%, it seems that Mn-Si oxides react with the support material, especially CaO, forming other components, weakening their CLOU properties. Their low CLOU oxygen release and low gas conversion as analyzed before may explain this.

Table. 5. Crystalline phases detected by X-ray diffraction for Mn-Si oxygen carriers supported by CaO.

Oxygen carrier	Fresh component	Used component
Mn44SiCa41-1100	Ca_2SiO_4, Mn_3O_4, $CaSiO_3$, $CaMn_2O4$	Ca_2SiO_4, Mn_3O_4, $CaSiO_3$, $CaMn_2O4$
Mn44SiCa41-1150	Ca_2SiO_4, Mn_3O_4	Ca_2SiO_4, Mn_3O_4
Mn44SiCa41-1200	Ca_2SiO_4, Mn_3O_4, SiO_2	-
Mn59SiCa21-1100	Ca_2SiO_4, Mn_3O_4, $CaSiO_3$, $CaMn_6(SiO_4)O_8$, $MnSiO_3$	Mn_3O_4, $CaSiO_3$, $MnSiO_3$
Mn59SiCa21-1150	$Mn_7(SiO_4)O_8$, $MnSiO_3$	Mn_3O_4, $CaSiO_3$
Mn59SiCa21-1200	Mn_3O_4, $CaSiO_3$	-
Mn71SiCa5-1100	$Mn_7(SiO_4)O_8$, $CaMn_2$+$2Si_3O_9$	$Mn_7(SiO_4)O_8$, Mn_3O_4, $CaSiO_3$, $CaMn_2$+$2Si_3O_9$
Mn71SiCa5-1150	$Mn_7(SiO_4)O_8$, $CaMn_2$+$2Si_3O_9$, Ca_2SiO_4	$Mn_7(SiO_4)O_8$, $CaMn_2$+$2Si_3O_9$, Ca_2SiO_4, Mn_3O_4
Mn71SiCa5-1200	$Mn_7(SiO_4)O_8$, $CaMn_2$+$2Si_3O_9$, Mn_3O_4, Mn_2O_3	$Mn_7(SiO_4)O_8$, $MnSiO_3$, Mn_3O_4, $Ca_{0.228}Mn_{0.772}SiO_3$
Mn74SiCa2-1100	$Mn_7(SiO_4)O_8$, $MnSiO_3$	$Mn_7(SiO_4)O_8$, $MnSiO_3$, Mn_3O_4
Mn74SiCa2-1150	$Mn_7(SiO_4)O_8$, $MnSiO_3$	$Mn_7(SiO_4)O_8$, $MnSiO_3$, Mn_3O_4
Mn74SiCa2-1200	$Mn_7(SiO_4)O_8$, $MnSiO_3$, Mn_2O_3, Ca_2SiO_4, $CaMn_4Si_5O_{15}$	$Mn_7(SiO_4)O_8$, $MnSiO_3$, Mn_3O_4, Ca_2SiO_4

Table. 6. Crystalline phases detected by X-ray diffraction for Mn-Si oxygen carriers supported by Al_2O_3.

Oxygen carrier	Fresh component	Used component
Mn48SiAl36-1100	$Mn_3Al_2(SiO_4)_3$, Mn_2AlO_4, $Mn_7(SiO_4)O_8$, SiO_2	$Mn_3Al_2(SiO_4)_3$, Mn_2AlO_4, SiO_2
Mn48SiAl36-1150	SiO_2, $Mn_3Al_2(SiO_4)_3$, Mn_2AlO_4	SiO_2, $Mn_3Al_2(SiO_4)_3$, Mn_2AlO_4
Mn48SiAl36-1200	$Mn_3Al_2(SiO_4)_3$, Mn_2AlO_4	-
Mn62SiAl17-1100	$Mn_7(SiO_4)O_8$, $Mn_3Al_2(SiO_4)_3$, SiO_2	$Mn_3Al_2(SiO_4)_3$, Mn_2AlO_4, SiO_2
Mn62SiAl17-1150	$Mn_7(SiO_4)O_8$, $Mn_3Al_2(SiO_4)_3$, Mn_2AlO_4, Mn_2O_3	$Mn_7(SiO_4)O_8$, $Mn_3Al_2(SiO_4)_3$, Mn_2AlO_4, Mn_2O_3
Mn69SiAl7-1150	$Mn_7(SiO_4)O_8$, $Mn_3Al_2(SiO_4)_3$	$Mn_3Al_2(SiO_4)_3$, $MnSiO_3$, Mn_3O_4
Mn72SiAl4-1100	$Mn_7(SiO_4)O_8$, SiO_2	$Mn_7(SiO_4)O_8$, $MnSiO_3$, Mn_3O_4
Mn72SiAl4-1150	$Mn_7(SiO_4)O_8$, $MnSiO_3$	$Mn_7(SiO_4)O_8$, $MnSiO_3$, Mn_3O_4
Mn72SiAl4-1200	$Mn_7(SiO_4)O_8$, $MnSiO_3$, Mn_3O_4	$Mn_7(SiO_4)O_8$, $MnSiO_3$, Mn_3O_4
Mn74SiAl2-1100	$Mn_7(SiO_4)O_8$, SiO_2, Mn_2O_3	$Mn_7(SiO_4)O_8$, $MnSiO_3$, Mn_3O_4
Mn74SiAl2-1150	$Mn_7(SiO_4)O_8$, $MnSiO_3$, Mn_3O_4	$Mn_7(SiO_4)O_8$, $MnSiO_3$, Mn_3O_4
Mn74SiAl2-1200	$Mn_7(SiO_4)O_8$, $MnSiO_3$	$Mn_7(SiO_4)O_8$, $MnSiO_3$, Mn_3O_4

3.5 Electron images (SEM)

To determine the changes in the oxygen carrier particles' structure before and after reactivity tests, electron images are taken with 1100 × magnification by scanning electron microscope (SEM), see Table. 7 to Table. 9. When comparing the images of oxygen carrier Mn48SiAl36-1150 with the images of the other two samples, it is obvious that the pore number on the particle Mn48SiAl36-1150 is much smaller. This observation shows that this oxygen carrier has less particle porosity indicating smaller surface area. Thus, the significantly bad CLOU behavior and low fuel conversion ability of the sample Mn48SiAl36-1150 which are illustrated in Fig. 9, Fig. 15 and Fig. 16 can be explained. In addition, no big difference can be recognized in the comparison between the images of fresh and used state for sample Mn72SiAl4-1150 and Mn74SiAl2-1150, see Table. 8 and Table. 9. A slight decrease of pore number can be seen in the sample Mn48SiAl36-1150 before and after usage, which interprets the decline of the fuel conversion ability shown in Fig. 17.

Table. 7. SEM images of Mn48SiAl36-1150 in fresh and used state.

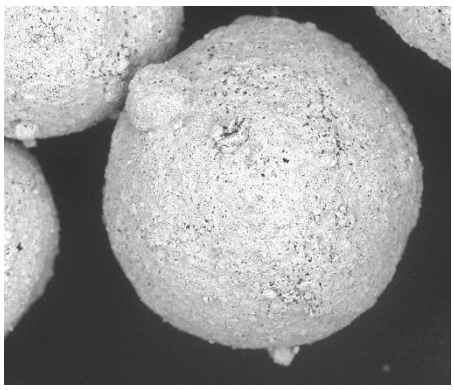
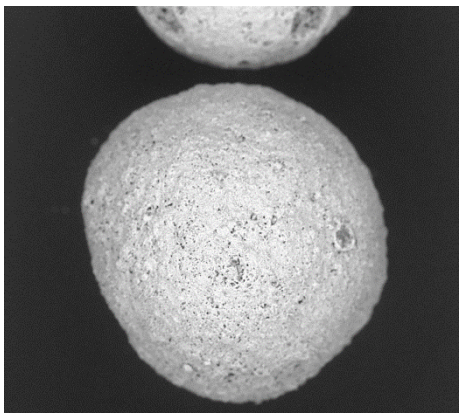
	Individual particle
Mn48SiAl36-1150 (fresh)	
Mn48SiAl36-1150 (used)	

Table. 8. SEM images of Mn72SiAl4-1150 in fresh and used state.

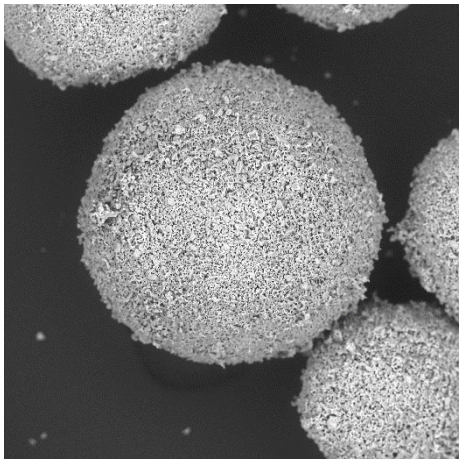
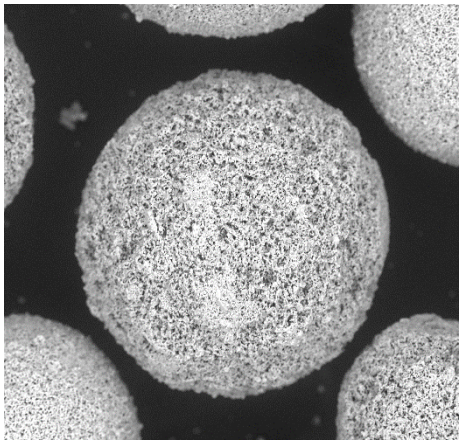
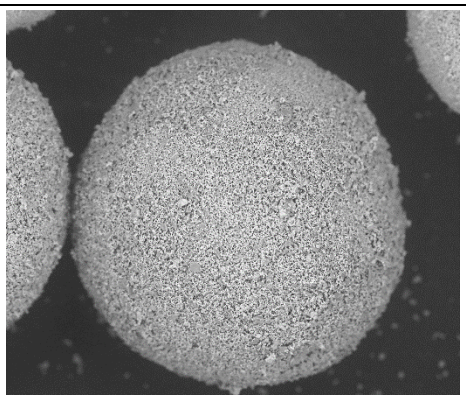
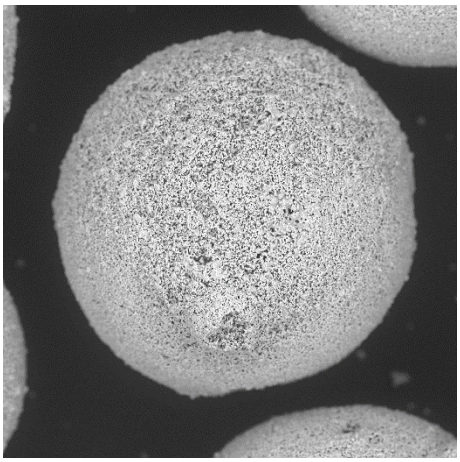
	Individual particle
Mn72SiAl4-1150 (fresh)	
Mn72SiAl4-1150 (used)	

Table. 9. SEM images of Mn74SiAl2-1150 in fresh and used state.

	Individual particle
Mn74SiAl2-1150 (fresh)	
Mn74SiAl2-1150 (used)	

4. Conclusions

Twenty-four oxygen carriers with different composition ratios, calcined from different temperatures, supported on two different supports are investigated in this study to identify the most feasible one to scale-up for industrial use.

All the Mn-Si oxides supported on CaO achieve almost full conversion of syngas to CO_2 and H_2O regardless of composition ratio and calcination temperature. However, regarding O_2 transport ability and the conversion towards methane, too high sintering temperature (1200 °C) becomes the main limiting factor. The performance of these oxygen carriers demonstrates an almost inversely proportional relationship to the CaO content. Mn71SiCa5-1100, Mn71SiCa5-1150, Mn74SiCa2-1100 and Mn74SiCa2-1150 show the best CLOU behavior.

Deactivation is detected for Mn71SiCa5-1200 and Mn74SiCa2-1200 when comparing the conversion results of the second operation in bed temperature 950 °C to the first one. No clear correlation between the mechanical strength and the nature of the oxides could be found. Among these samples, Mn71SiCa5-1100 can be regarded as the best candidate which exhibits rather good CLOU property, outstanding reactivity and show comparatively high long-term durability.

For the Mn-Si oxygen carries with Al_2O_3 as support material, the production process becomes more important for the performance. In addition, the oxides tend to display better CLOU behavior with lower Al_2O_3 content. Mn48SiAl36 calcined from 1200 °C shows exceptionally low conversion towards both syngas and methane. Mn72SiAl4-1100, Mn74SiAl2-1100 and Mn74SiAl2-1150 still show remarkable capacity to convert methane. Unlike the samples supported by CaO, deactivation occurs for some samples supported on Al_2O_3 after undergoing the strongest operation condition (1050 °C), especially Mn62SiAl17-1150, Mn72SiAl4-1200 and Mn74SiAl2-1200. The higher calcination temperature contributes to the better mechanical property, which can be interpreted by more resistance to attrition and higher crushing strength. Mn72SiAl4-1100 is the best oxygen carrier in comparison with other eleven Al-based samples. In addition, higher bed temperatures facilitate the performance of all twenty-four oxygen carriers.

Mn71SiCa5-1100 and Mn72SiAl4-1100 are the most interesting oxygen carriers that deserve further examination. Both of them show noteworthy oxygen release ability. And they also show almost full conversion of syngas and significant ability to convert methane. However, when considering their mechanical characteristics, Mn72SiAl4-1100 is more robust when the calcination temperatures fluctuate.

5. Reference

Adanez, J. A. A. G.-L. F. G. P. &. d. D. L., 2012. Progress in Chemical-Looping Combustion and Reforming technologies. *Progress in Energy and Combustion Science*, 38(2), pp. 215-282.

Arjmand, M. A. A. L. H. M. T. L. A., 2012. Evaluation of CuAl2O4 as an Oxygen Carrier in Chemical-Looping Combustion. *Industrial & Engineering Chemistry Research*, 51(43).

Azimi, G. L. H. R. M. M. T. L. A., 2012. Investigation of different Mn–Fe oxides as oxygen carrier for chemical-looping with oxygen uncoupling (CLOU). *Energy & Fuels*, 27(1), p. 367.

Fan, J. Z. L. J. P. L. L. &. L. H., 2016. Comparative exergy analysis of chemical looping combustion thermally coupled and conventional steam methane reforming for hydrogen production. *Journal of Cleaner Production*, vol 131, pp. 247-258.

Frick, V. R. M. L. H., 2016. Investigation of Cu–Fe and Mn–Ni oxides as oxygen carriers for chemical-looping combustion. *Fuel Processing Technology*, vol 150, pp. 30-40.

Frick, V. R. M. L. H. M. T. L. A., 2015. Screening of supported and unsupported Mn–Si oxygen carriers for CLOU (chemical-looping with oxygen uncoupling). *Energy*, vol 93, pp. 544-554.

Galina A. Bukhtiyarova, I. V. D. S. S. V. K. M. P. I. B., 2007. Effect of the calcination temperature on the properties of Fe2O3/SiO2 catalysts for oxidation of hydrogen sulfide. *Reaction Kinetics and Catalysis Letters*, vol 92, pp. 89-97.

García-Labiano, F. d. D. L. G. P. A. J. A. A. &. D. C., 2009. Effect of Fuel Gas Composition in Chemical-Looping Combustion with Ni-Based Oxygen Carriers. 1. Fate of Sulfur. *Industrial & Engineering Chemistry Research*, 48(5), pp. 2499-2508.

Ge, H. S. L. G. H. S. T. &. J. S., 2016. Combustion performance and sodium absorption of ZhunDong coal in a CLC process with hematite oxygen carrier. *Applied Thermal Engineering*, vol 94, pp. 40-49.

HARPER, F., 1967. Effect of calcination temperature on properties of magnesium oxides for use in magnesium oxychloride cements. *Journal of applied chemistry*, 17(1), p. 5.

J. Adánez, L. F. d. D. F. G.-L. P. G. a. A. A., 2004. Selection of Oxygen Carriers for Chemical-Looping Combustion. *Energy & Fuels*, 18(2), pp. 371-377.

Jabbary, F., 2014. Comparison of nickel and iron-based oxygen carriers supported on alumina in syngas-fueled chemical looping combustion. *ProQuest Dissertations Publishing*.

Jerndal, E. L. H. A. L. E. T. H. M. J. K. K. M. S. R. M. T. &. L. A., 2011. Using Low-Cost Iron-Based Materials as Oxygen Carriers for Chemical Looping Combustion. *Oil & Gas Science and Technology – Revue d'IFP Energies nouvelles*, 66(2), pp. 235-248.

Jing, D. A. M. M. T. R. M. S. F. L. H. L. A., 2014. Examination of oxygen uncoupling behaviour and reactivity towards methane for manganese silicate oxygen carriers in chemical-looping combustion. *International Journal of Greenhouse Gas Control*, vol 29, pp. 70-81.

Jing, D. M. T. L. H. R. M. &. L. A., 2013. Examination of Perovskite Structure CaMnO3-δwith MgO Addition as Oxygen Carrier for Chemical Looping with Oxygen Uncoupling Using Methane and Syngas. *International Journal of Chemical Engineering*, vol 2013, pp. 1-16.

Källén, M. R. M. M. T. L. A., 2014. Operation with Combined Oxides of Manganese and Silica as Oxygen Carriers in a 300 Wth Chemical-looping Combustion Unit. *Energy Procedia*, vol 63, pp. 131-139.

Kale, G., 2012. Feasibility study of sulfates as oxygen carriers for chemical looping processes. *QScience Connect*, vol 2012, p. 2012.

Kanniche, M. G.-B. R. J. P. V.-M. J. A. J. &. B. C., 2010. Pre-combustion, post-combustion and oxy-combustion in thermal power plant for CO2 capture. *Applied Thermal Engineering*, 30(1), pp. 53-62.

Keller, M. A. M. L. H. M. T., 2014. Interaction of mineral matter of coal with oxygen carriers in chemical-looping combustion (CLC). *Chemical Engineering Research and Design*, 92(9), pp. 1753-1770.

Leion, H. L. A. M. T., 2009. Solid fuels in chemical-looping combustion using a NiO-based oxygen carrier. *Chemical Engineering Research and Design*, 87(11), p. 1543–1550.

Leion, H. M. T. &. L. A., 2009. Using chemical-looping with oxygen uncoupling (CLOU) for combustion six different of solid fuels. *Energy Procedia*, 1(1), p. 447–453.

Lenton, T., 2011. 2[degrees]C or not 2[degrees]C? That is the climate question: targets to limit the global temperature rise won't prevent climate disruption. Tim Lenton says that policy-makers should focus on regional impacts. *Nature*, 473(7345), p. 7.

Linderholm, C. M. T. &. L. A., 2009. Long-term integrity testing of spray-dried particles in a 10-kW chemical-looping combustor using natural gas as fuel. *Fuel*, 88(11), p. 2083–2096.

Lyngfelt, A., 2014. Chemical-looping combustion of solid fuels – Status of development. *Applied Energy*, vol 113, pp. 1869-1873.

Lyngfelt, A. L. B. M. T., 2001. A fluidized-bed combustion process with inherent CO2 separation; application of chemical-looping combustion. *Chemical Engineering Science*, 56(10), pp. 3101-3113.

Mattisson, T. L. H. L. A., 2009. Chemical-looping with oxygen uncoupling using CuO/ZrO2 with petroleum coke. *Fuel*, 88(4), pp. 683-690.

Mohammad Pour, N. L. H. R. M. M. T., 2013. Combined Cu/Mn Oxides as an Oxygen Carrier in Chemical Looping with Oxygen Uncoupling (CLOU). *Energy & Fuels*, 27(10), p. 6031.

Pilar Gayán, C. R. F. A. A. L. F. d. D. F. G.-L. a. J. A., 2011. Effect of Support on the Behavior of Cu-Based Oxygen Carriers during Long-Term CLC Operation at Temperatures above 1073 K. *Energy & Fuels*, 25(3), pp. 1316-1326.

Rydén, M. J. D. K. M. L. H. L. A. M. T., 2014. CuO-Based Oxygen-Carrier Particles for Chemical-Looping with Oxygen Uncoupling - Experiments in Batch Reactor and in Continuous Operation. *Industrial & Engineering Chemistry Research*, 53(15), p. 6255.

Rydén, M. L. H. M. T. L. A., 2014. Combined oxides as oxygen-carrier material for chemical-looping with oxygen uncoupling. *Applied Energy*, vol 113, pp. 1924-1932.

Rydén, M. M. P. L. S. M. T. L. A., 2014. Measuring attrition resistance of oxygen carrier particles for chemical looping combustion with a customized jet cup. *Powder Technology*, vol 256, pp. 75-86.

Shulman, A. C. E. M. T. L. A., 2011. Chemical – Looping with oxygen uncoupling using Mn/Mg-based oxygen carriers – Oxygen release and reactivity with methane. *Fuel*, 90(3), pp. 941-950.

Shulman, A. M. T. L. A., 2009. Manganese/iron, manganese/nickel, and manganese/silicon oxides used in chemical-looping with oxygen uncoupling (CLOU) for combustion of methane. *Energy & Fuels*, 23(10), p. 5269.

Siriwardane, R. T. H. M. D. &. R. G., 2015. Fluidized bed testing of commercially prepared MgO-promoted hematite and CuO–Fe2O3 mixed metal oxide oxygen carriers for methane and coal chemical looping combustion. *Applied Energy*, vol 157, pp. 348-357.

Sundqvist, S. A. M. M. T. R. M. &. L. A., 2015. Screening of different manganese ores for chemical-looping combustion (CLC) and chemical-looping with oxygen uncoupling (CLOU). *International Journal of Greenhouse Gas Control*, vol 43, pp. 179-188.

Tian, H. G. Q. Y. X. &. L. Y., 2010. Investigation into sulfur release in reductive decomposition of calcium sulfate oxygen carrier by hydrogen and carbon monoxide. *Fuel Processing Technology*, 91(11), pp. 1640-1649.

Toftegaard, M. B. J. J. P. G. P. &. J. A., 2010. Oxy-fuel combustion of solid fuels. *Progress in Energy and Combustion Science*, 36(5), pp. 581-625.

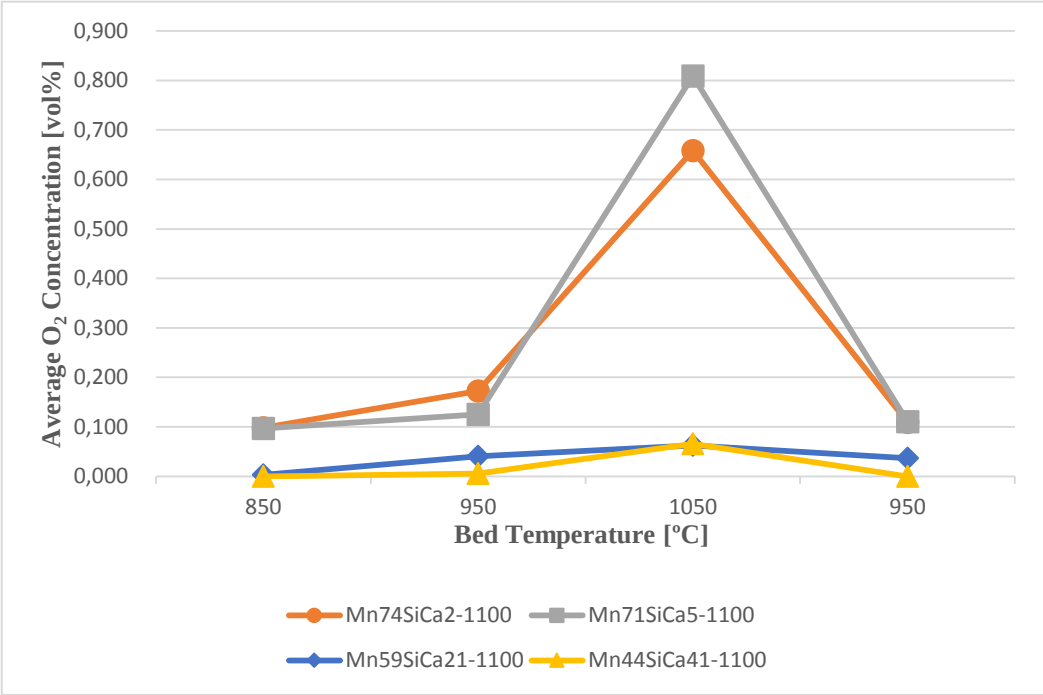
Wang, K. Y. Q. Q. Q. &. Z. Z., 2015. Analysis of oxygen releasing rate of Cu-based oxygen carrier in N2–O2 atmosphere. *Journal of Thermal Analysis and Calorimetry*, 119(3), pp. 2221-2227.

Zafar, Q. A. A. M. T. G. B. &. S. M., 2007. Reduction and oxidation kinetics of Mn3O4/Mg–ZrO2 oxygen carrier particles for chemical-looping combustion. *Chemical Engineering Science*, 62(33), pp. 6556-6567.

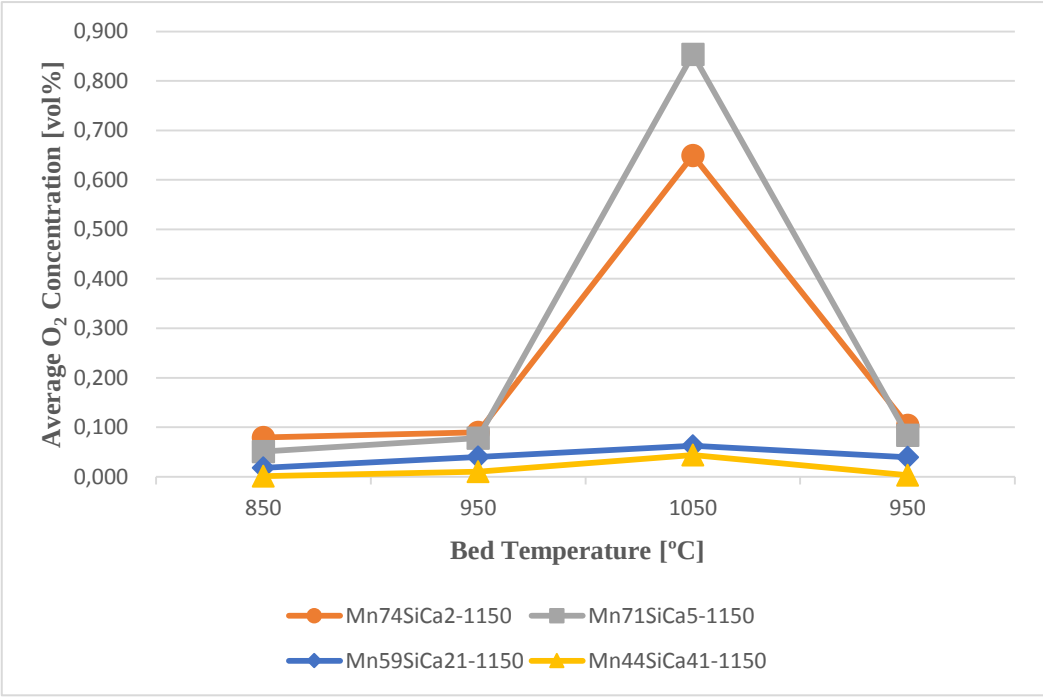
Zhao, H. C. Y. K. Z. W. Y. &. P. W., 2012. Thermal characteristics of Cu-based oxygen carriers. *Journal of Thermal Analysis and Calorimetry*, 109(3), pp. 1105-1109.

6. Appendix

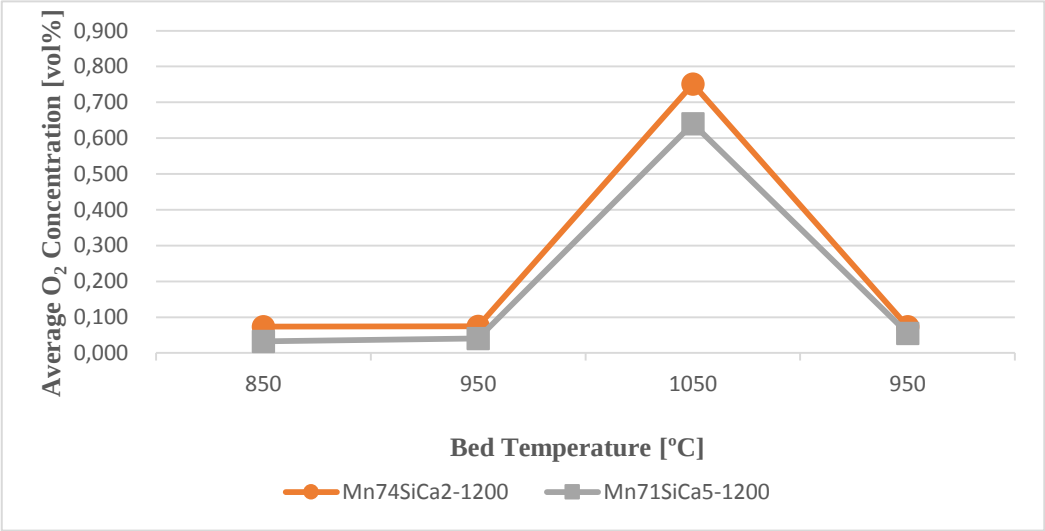
6.1 CLOU oxygen release



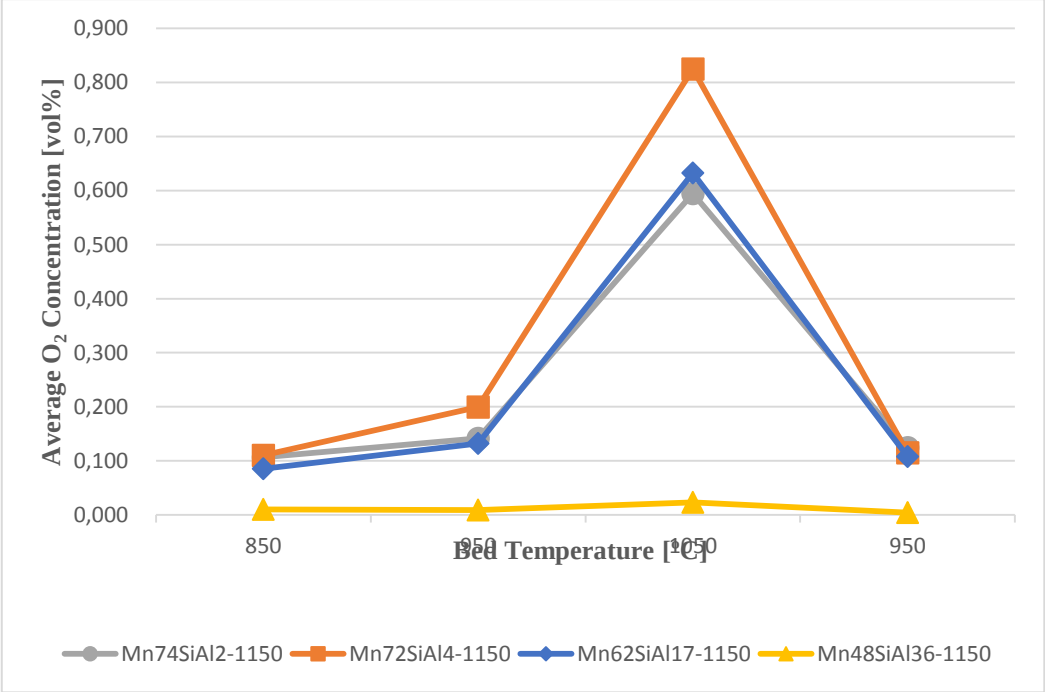
A 1. Average O_2 concentration during inert period for Mn-Si oxygen carriers calcined from 1100 °C supported by CaO.



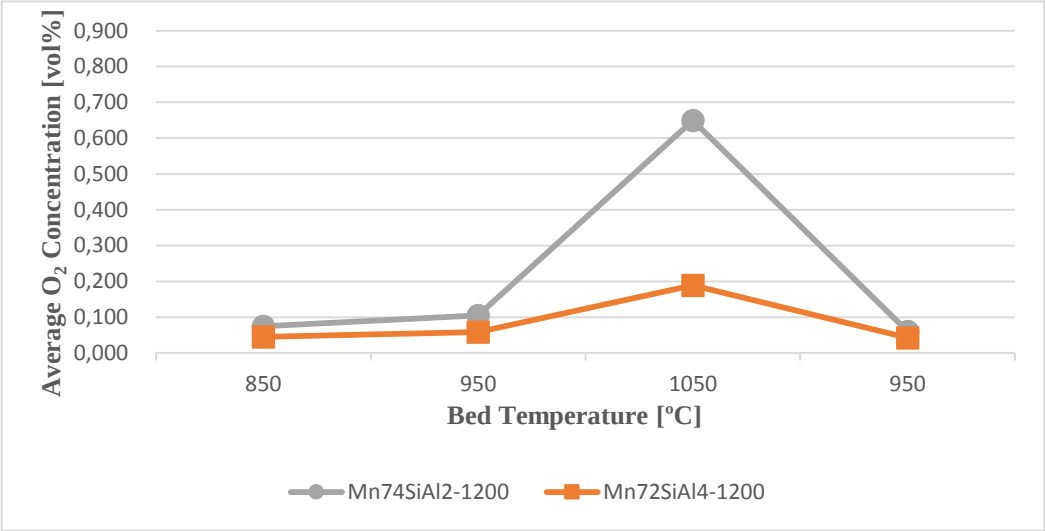
A 2. Average O_2 concentration during inert period for Mn-Si oxygen carriers calcined from 1150 °C supported by CaO.



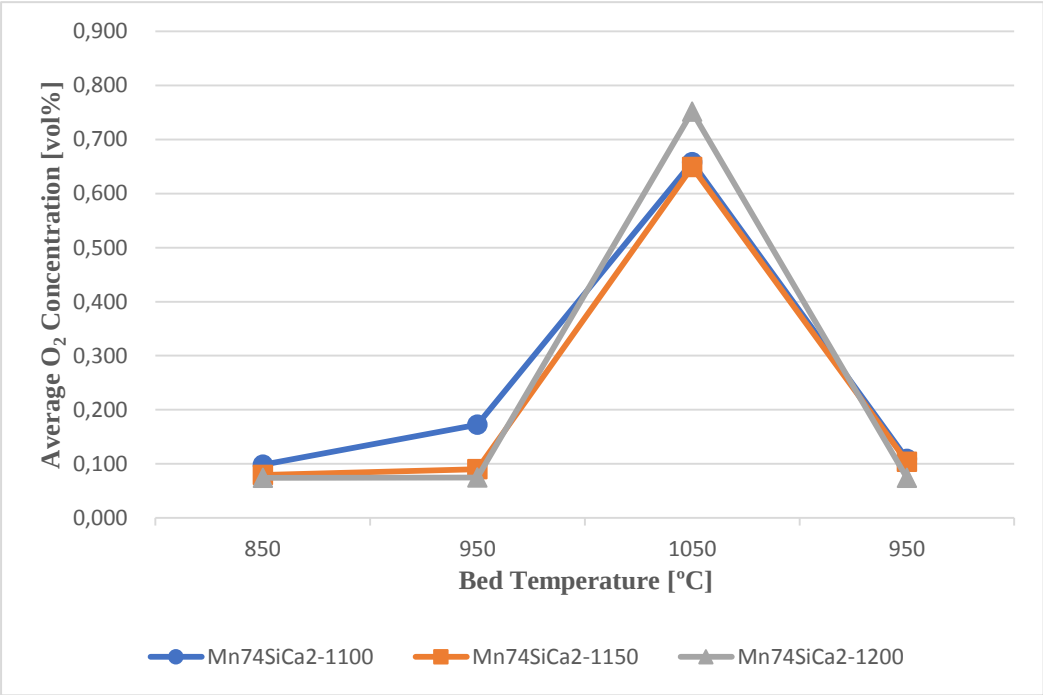
A 3. Average O_2 concentration during inert period for Mn-Si oxygen carriers calcined from 1200 °C supported by CaO.



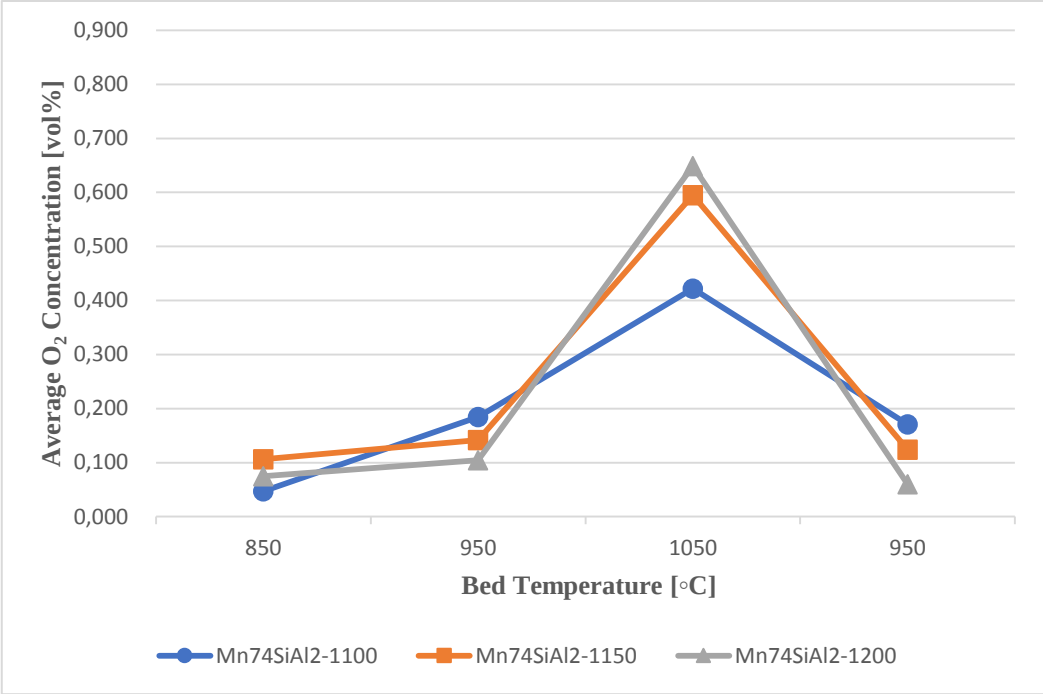
A 4. Average O_2 concentration during inert period for Mn-Si oxygen carriers calcined from 1150 °C supported by Al_2O_3.



A 5. Average O_2 concentration during inert period for Mn-Si oxygen carriers calcined from 1200 °C supported by Al_2O_3.

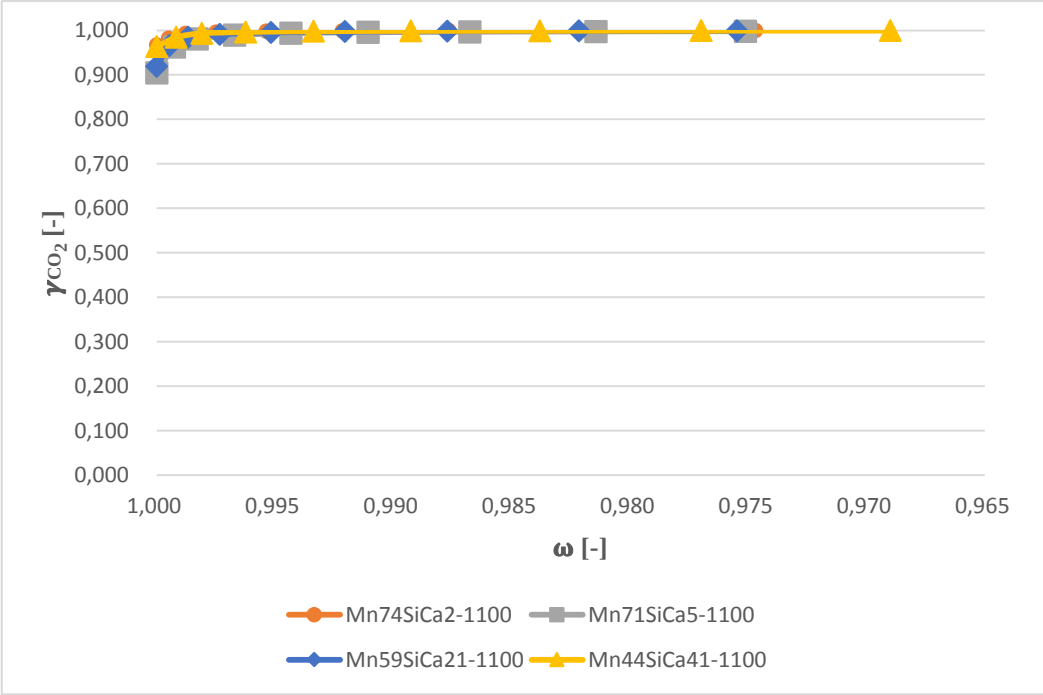


A 6. Average O_2 concentration during inert period for Mn74SiCa2 calcined in three temperatures.

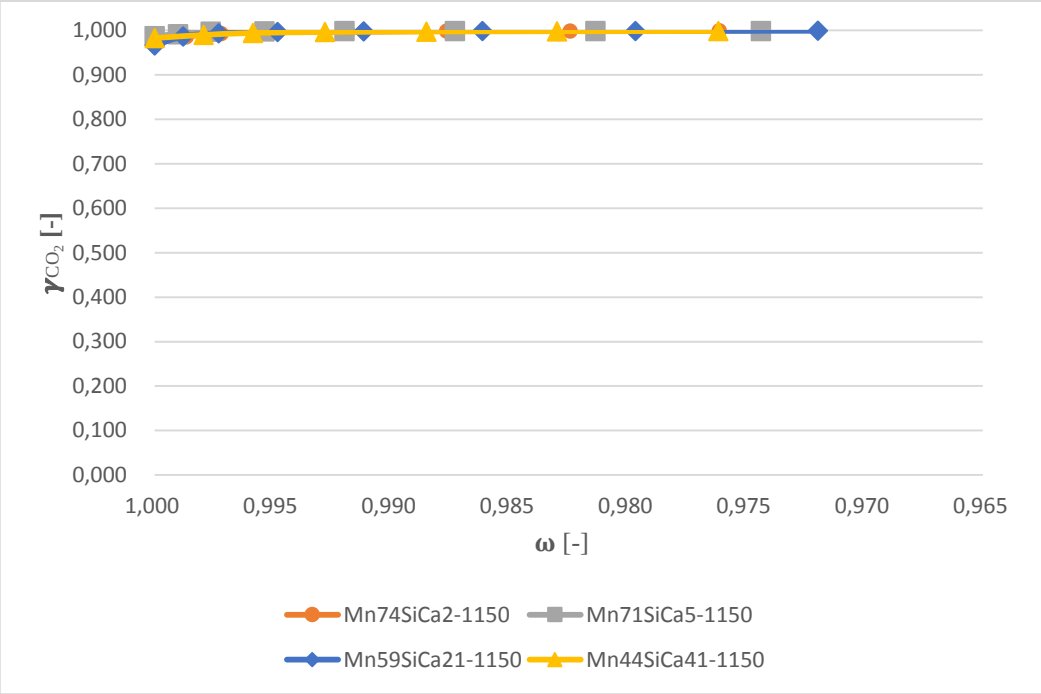


A 7. Average O_2 concentration during inert period for Mn74SiAl2 calcined in two temperatures.

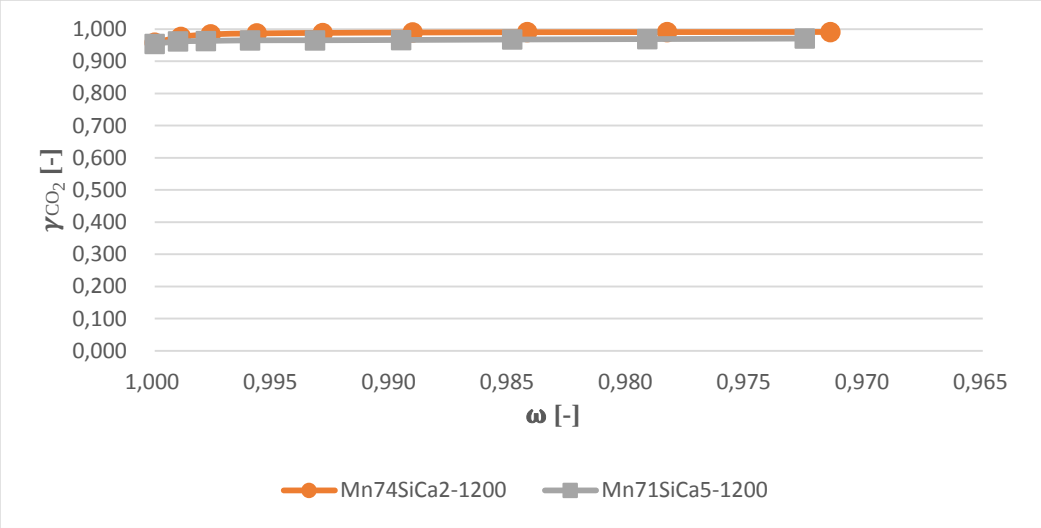
6.2 Fuel conversion



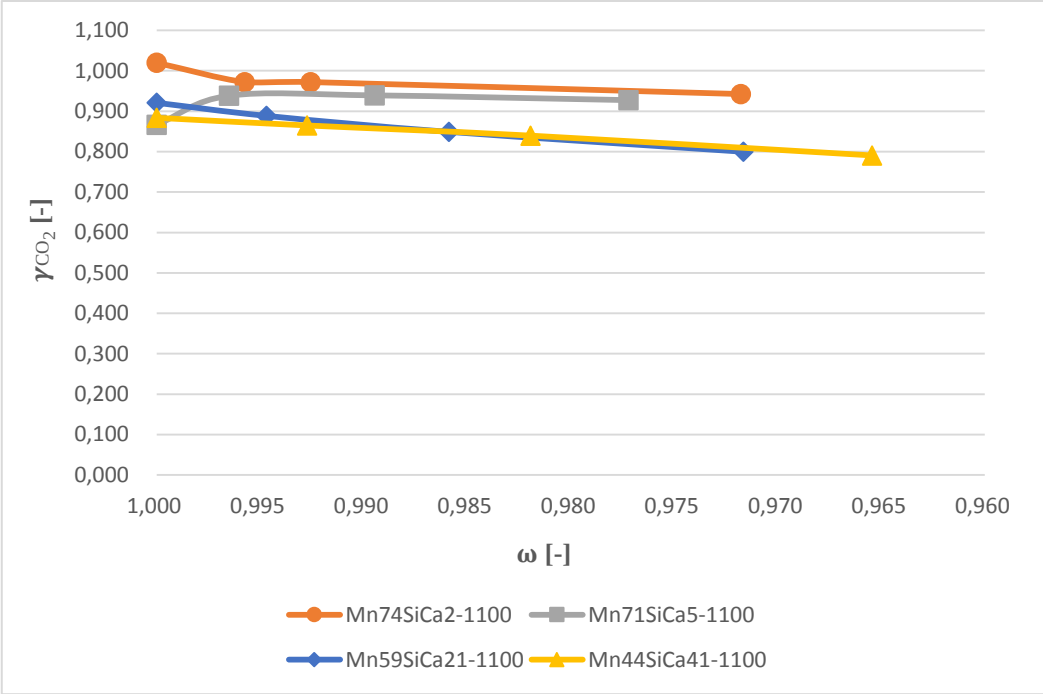
A 8. CO_2 yield as a function of oxygen carrier conversion of syngas at 950 °C for Mn-Si oxygen carriers calcined from 1100 °C supported by CaO.



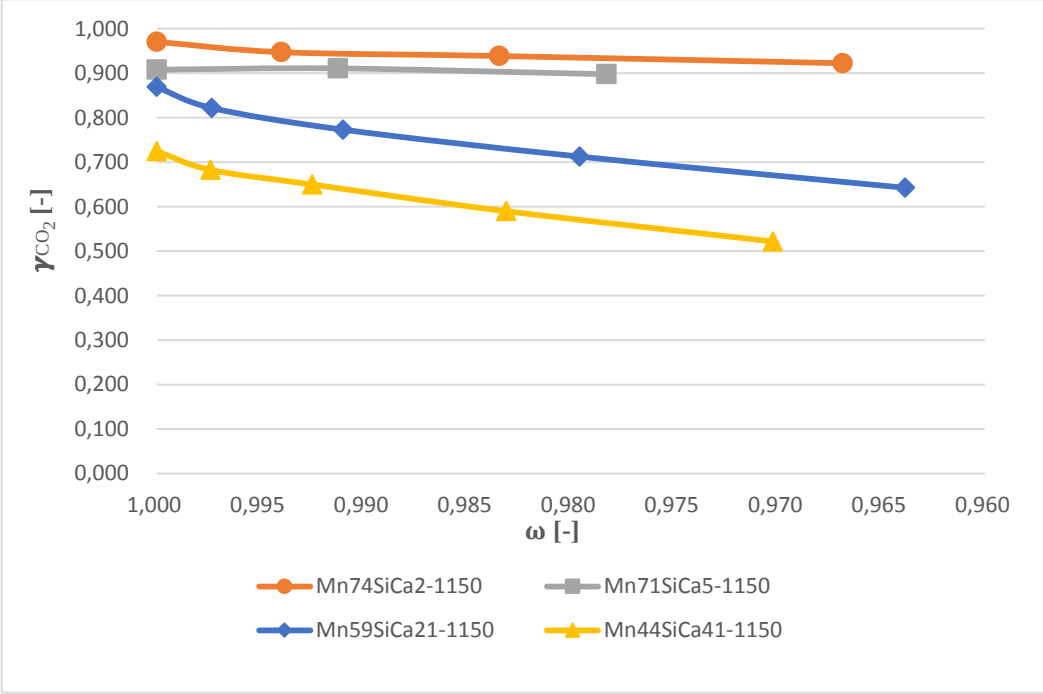
A 9. CO_2 yield as a function of oxygen carrier conversion of syngas at 950 °C for Mn-Si oxygen carriers calcined from 1150 °C supported by CaO.



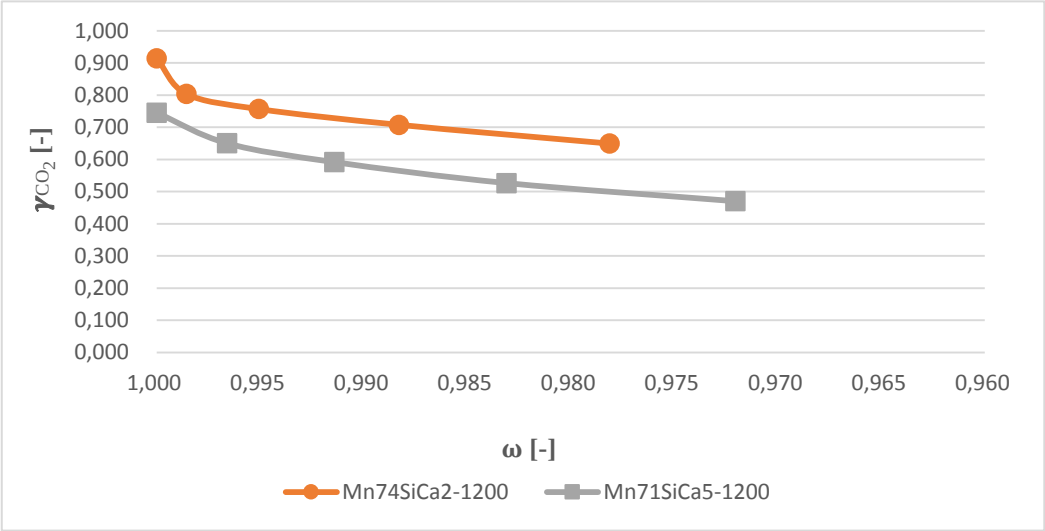
A 10. CO_2 yield as a function of oxygen carrier conversion of syngas at 950 °C for Mn-Si oxygen carriers calcined from 1200 °C supported by CaO.



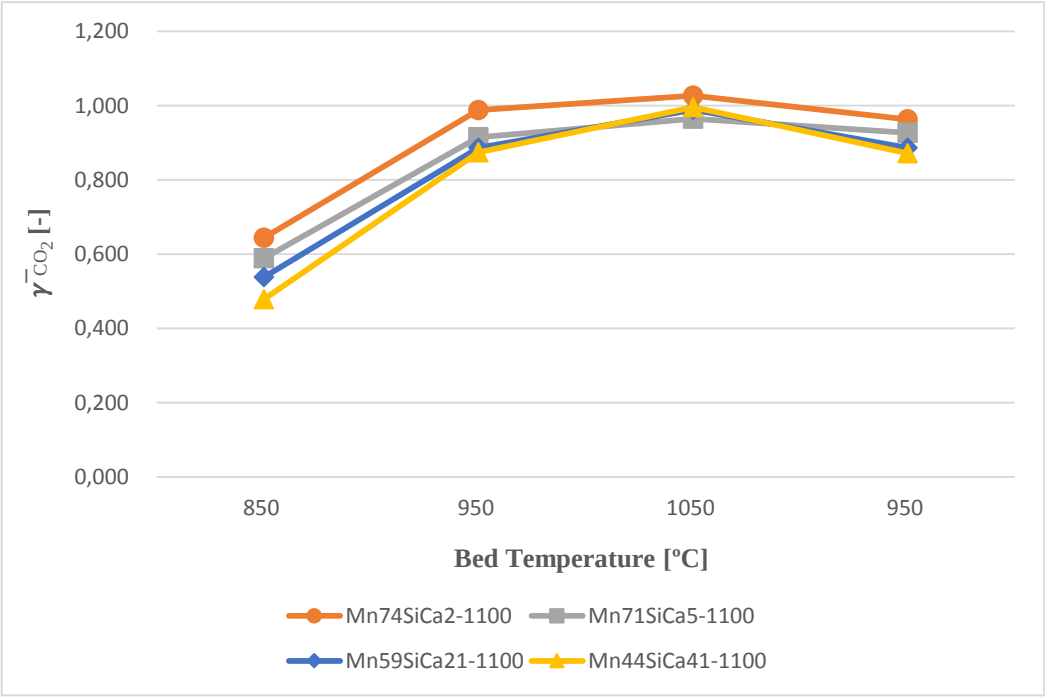
A 11. CO_2 yield as a function of oxygen carrier conversion of methane at 950 °C for Mn-Si oxygen carriers calcined from 1100 °C supported by CaO.



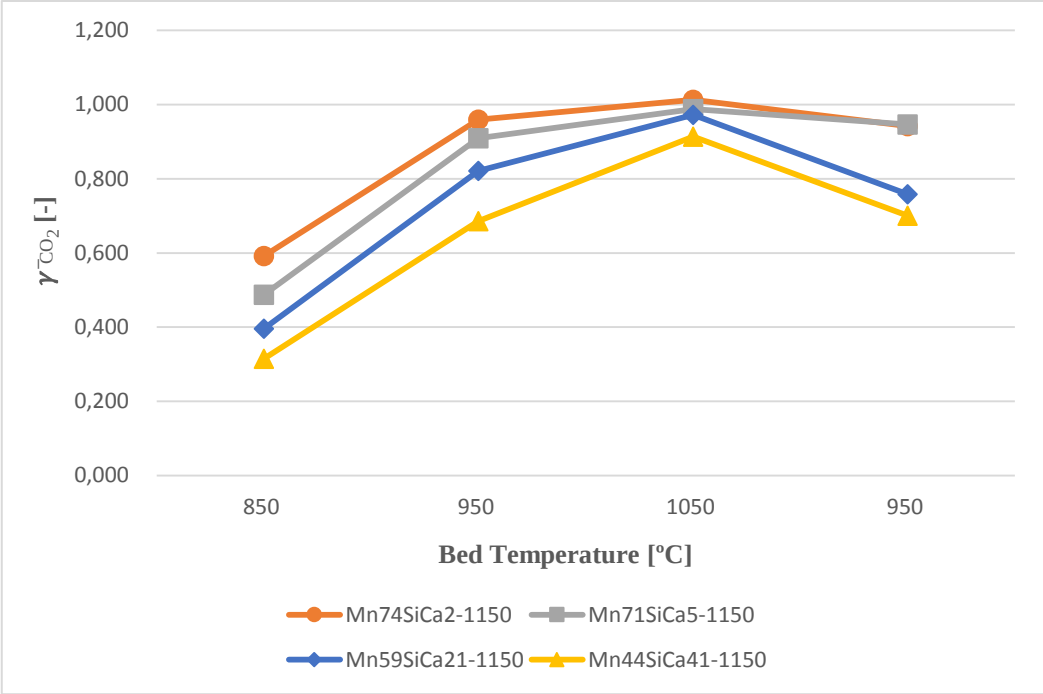
A 12. CO_2 yield as a function of oxygen carrier conversion of methane at 950 °C for Mn-Si oxygen carriers calcined from 1150 °C supported by CaO.



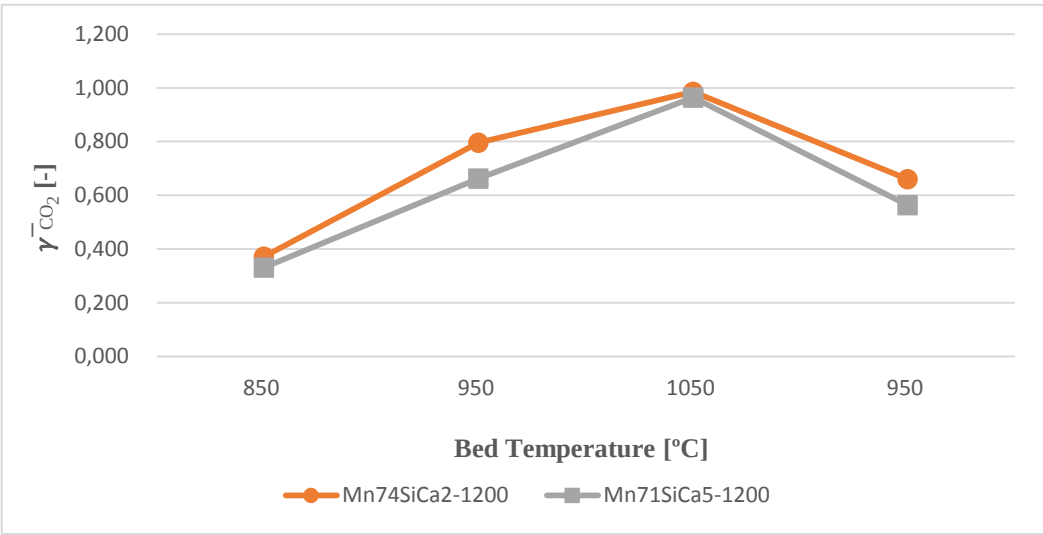
A 13. CO_2 yield as a function of oxygen carrier conversion of methane at 950 °C for Mn-Si oxygen carriers calcined from 1200 °C supported by CaO.



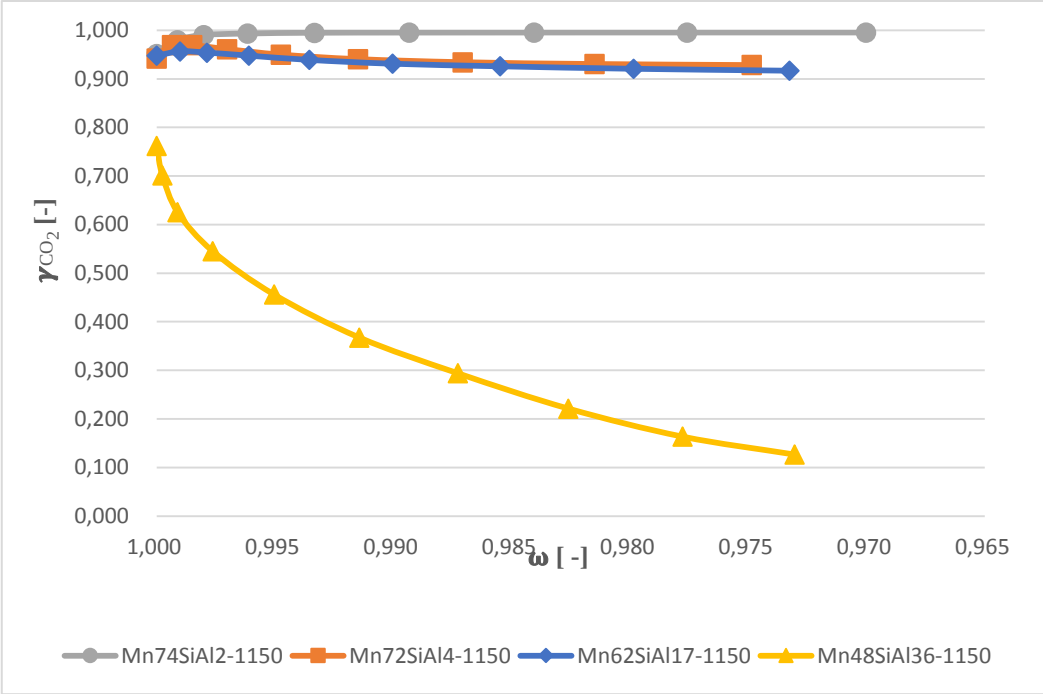
A 14. Average CO_2 yield as a function of the bed temperature of methane at 950 °C for Mn-Si oxygen carriers calcined from 1100 °C supported by CaO.



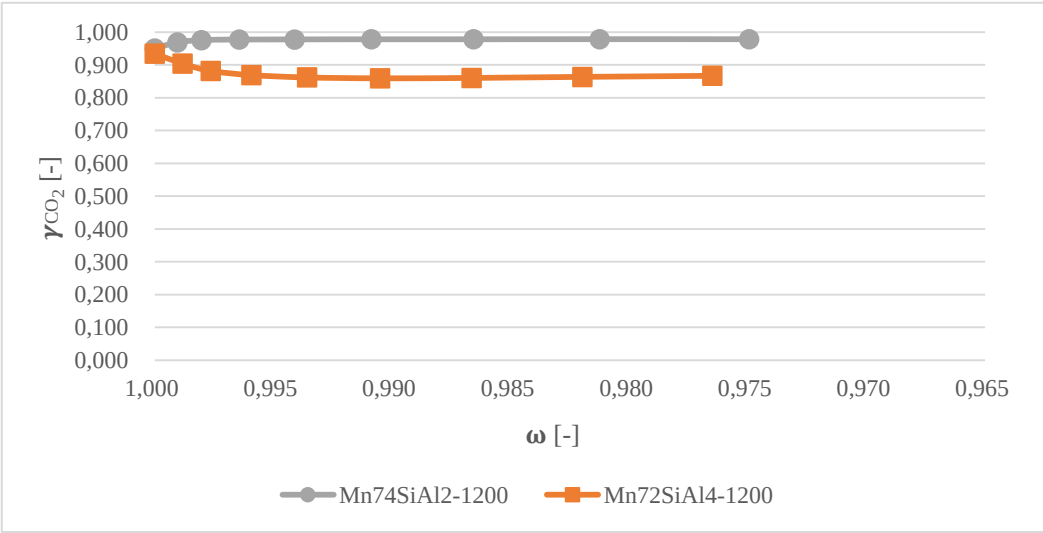
A 15. Average CO_2 yield as a function of the bed temperature of methane at 950 °C for Mn-Si oxygen carriers calcined from 1150 °C supported by CaO.



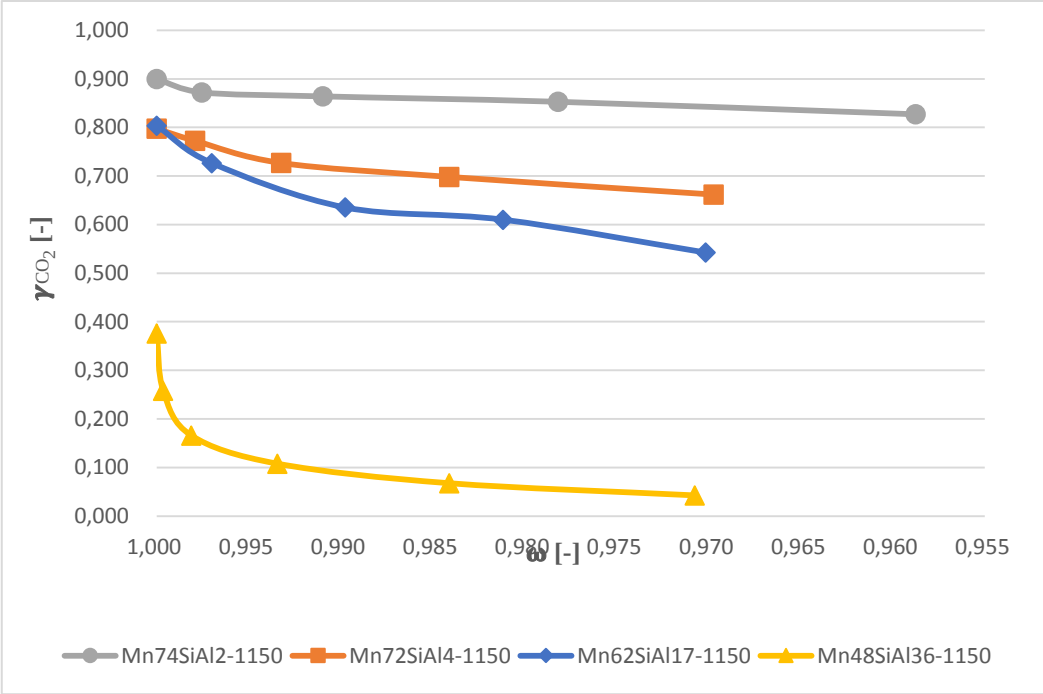
A 16. Average CO_2 yield as a function of the bed temperature of methane at 950 °C for Mn-Si oxygen carriers calcined from 1200 °C supported by CaO.



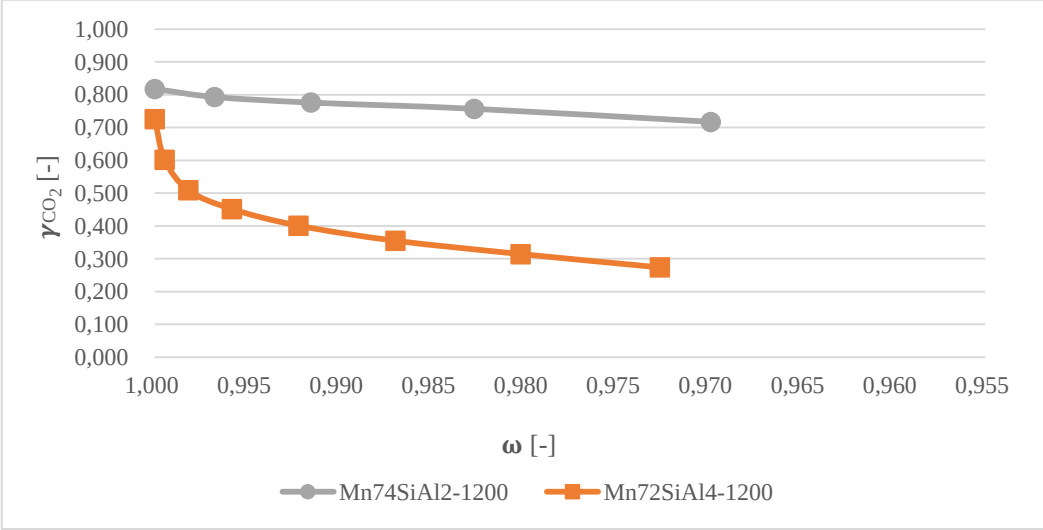
A 17. CO_2 yield as a function of oxygen carrier conversion of syngas at 950 °C for Mn-Si oxygen carriers calcined from 1150 °C supported by Al_2O_3.



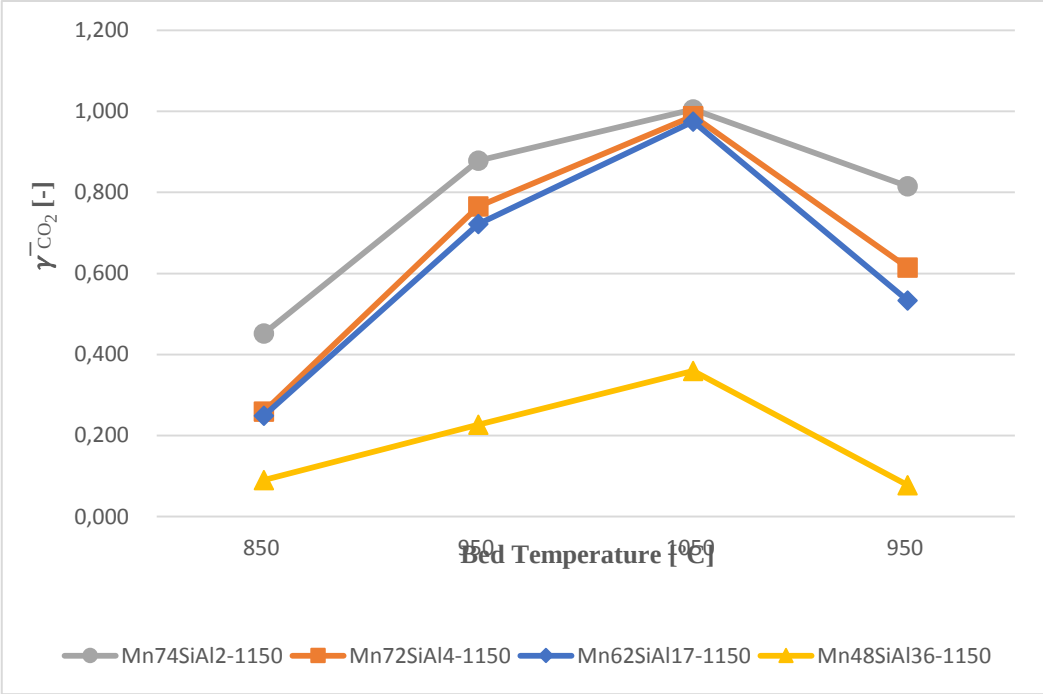
A 18. CO_2 yield as a function of oxygen carrier conversion of syngas at 950 °C for Mn-Si oxygen carriers calcined from 1200 °C supported by Al_2O_3.



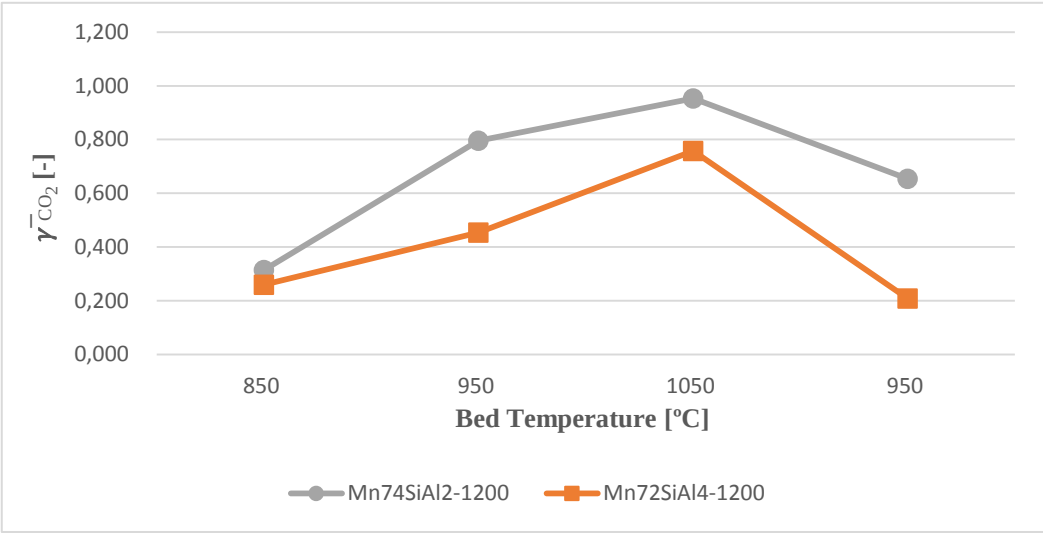
A 19. CO_2 yield as a function of oxygen carrier conversion of methane at 950 °C for Mn-Si oxygen carriers calcined from 1150 °C supported by Al_2O_3.



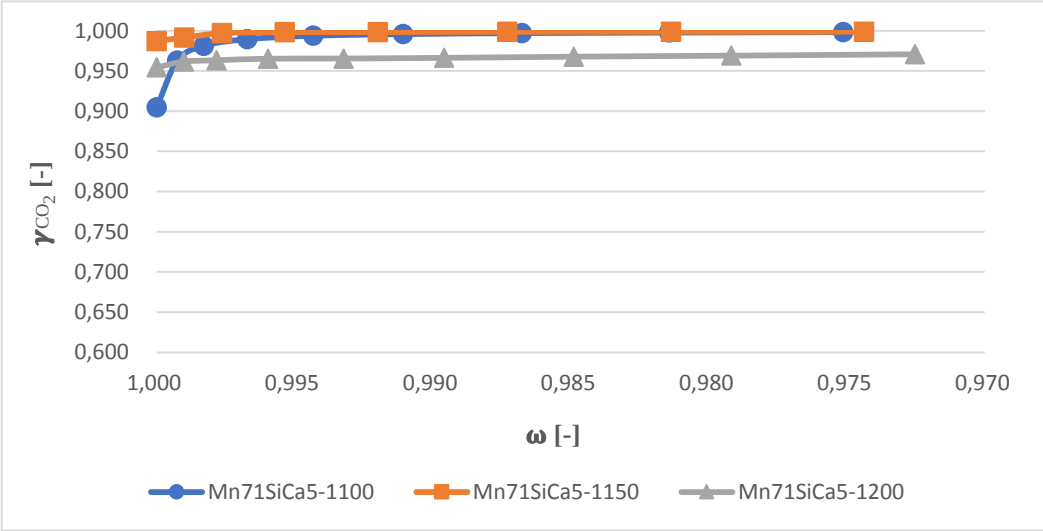
A 20. CO_2 yield as a function of oxygen carrier conversion of methane at 950 °C for Mn-Si oxygen carriers calcined from 1200 °C supported by Al_2O_3.



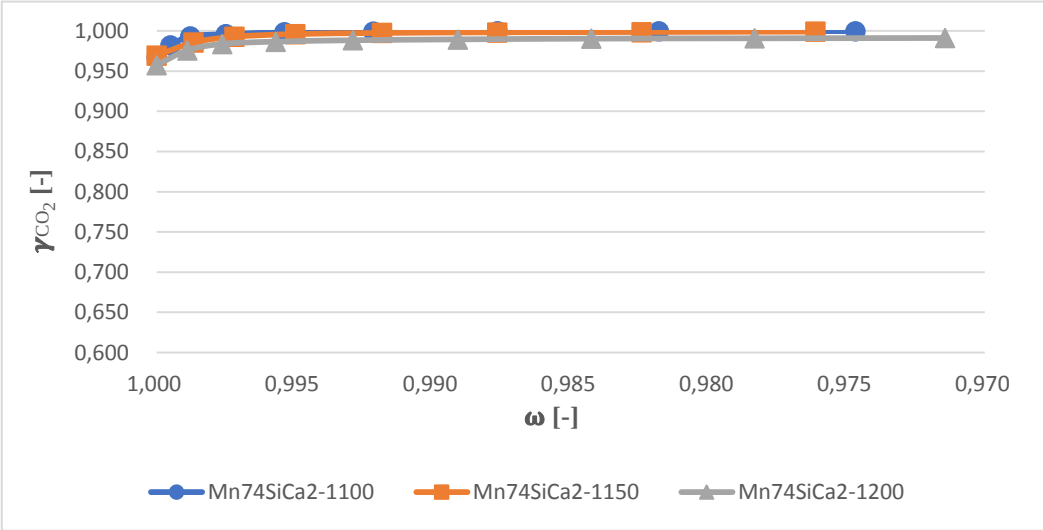
A 21. Average CO_2 yield as a function of the bed temperature of methane at 950 °C for Mn-Si oxygen carriers calcined from 1150 °C supported by Al_2O_3.



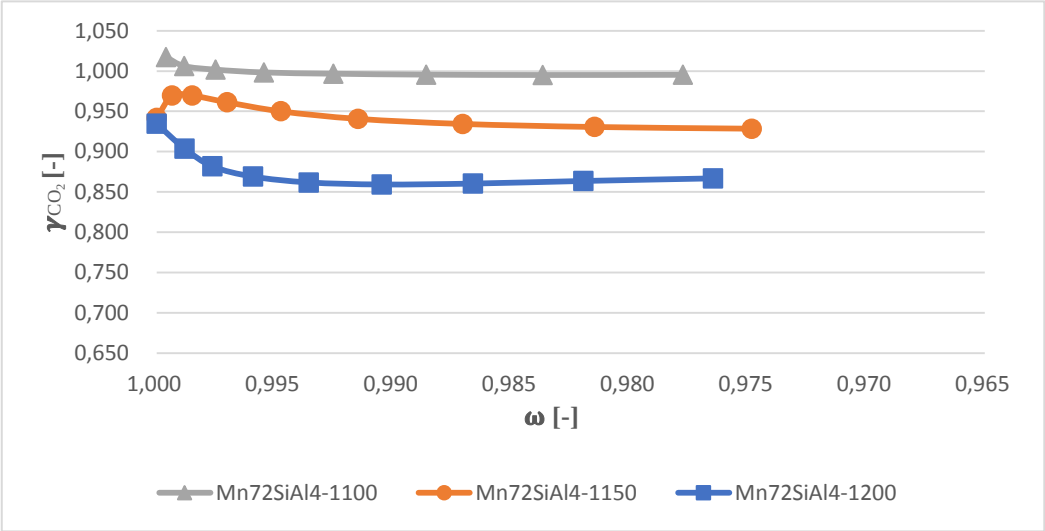
A 22. Average CO_2 yield as a function of the bed temperature of methane at 950 °C for Mn-Si oxygen carriers calcined from 1200 °C supported by Al_2O_3.



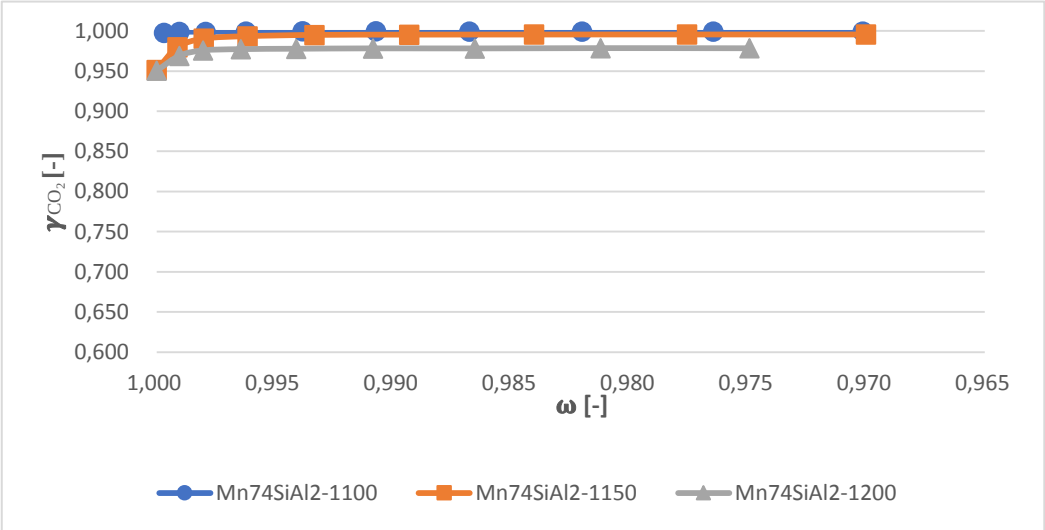
A 23. CO_2 yield as a function of oxygen carrier conversion of syngas for Mn71SiCa5 calcined in three temperatures.



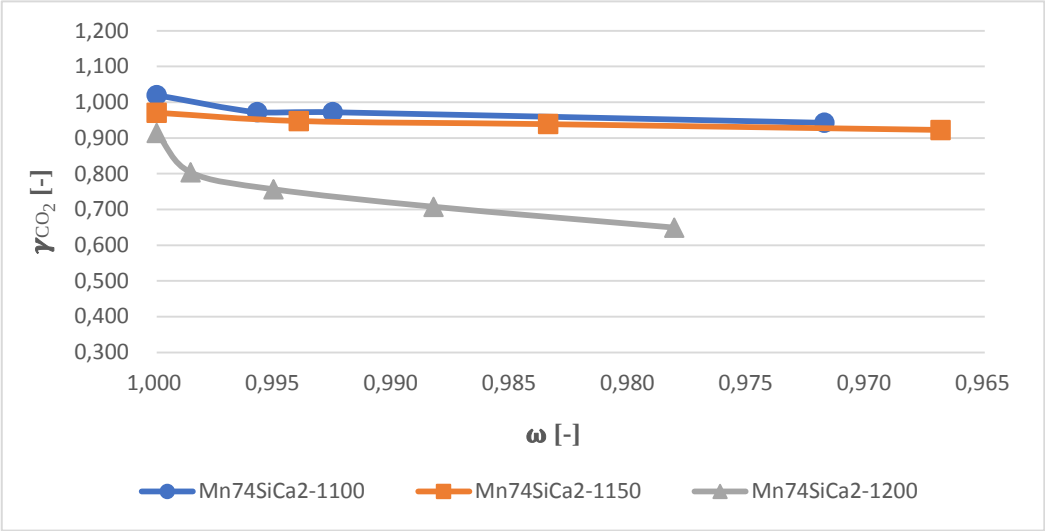
A 24. Average CO_2 yield as a function of oxygen carrier conversion of syngas for Mn74SiCa2 calcined in three temperatures.



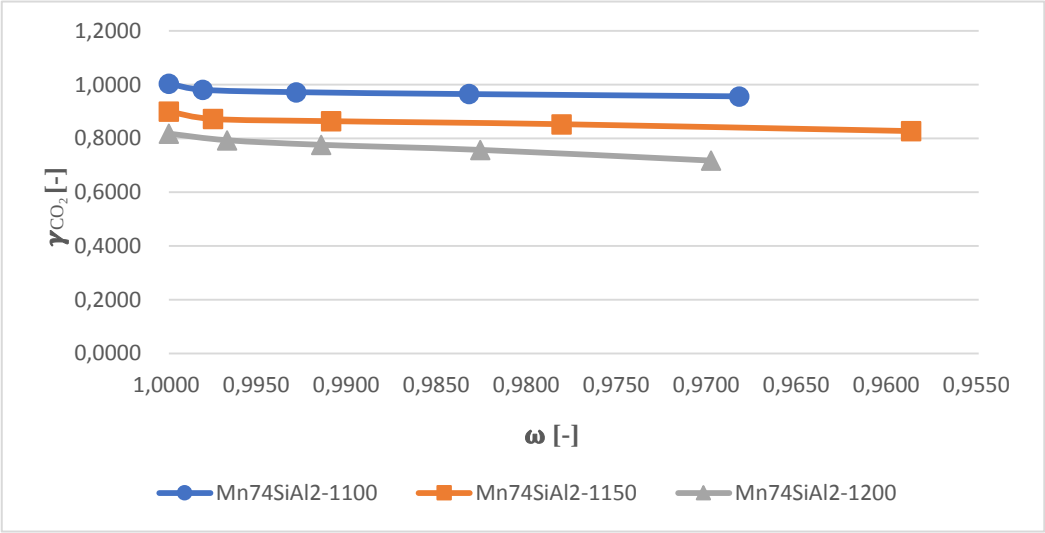
A 25. CO_2 yield as a function of oxygen carrier conversion of syngas for Mn72SiAl4 calcined in three temperatures.



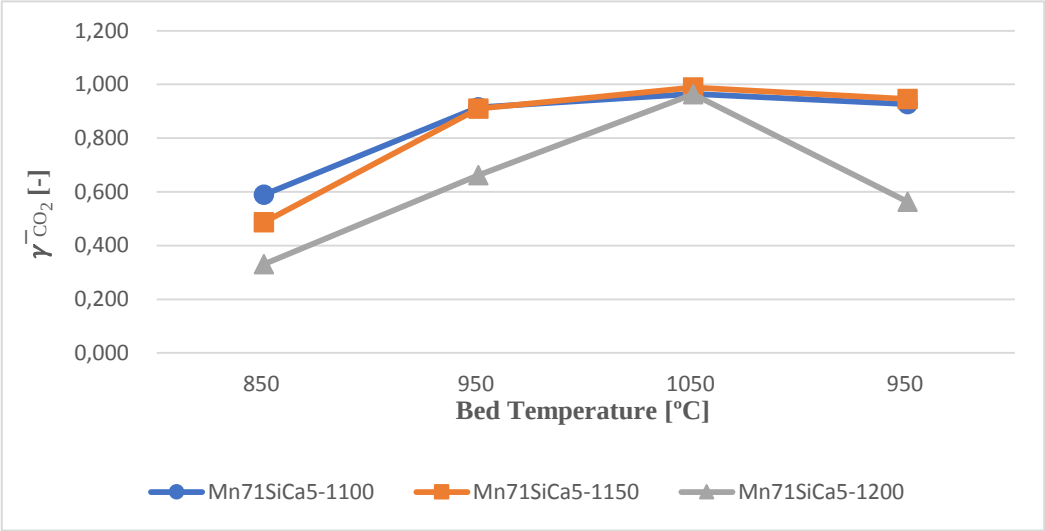
A 26. CO_2 yield as a function of oxygen carrier conversion of syngas for Mn74SiAl2 calcined in three temperatures.



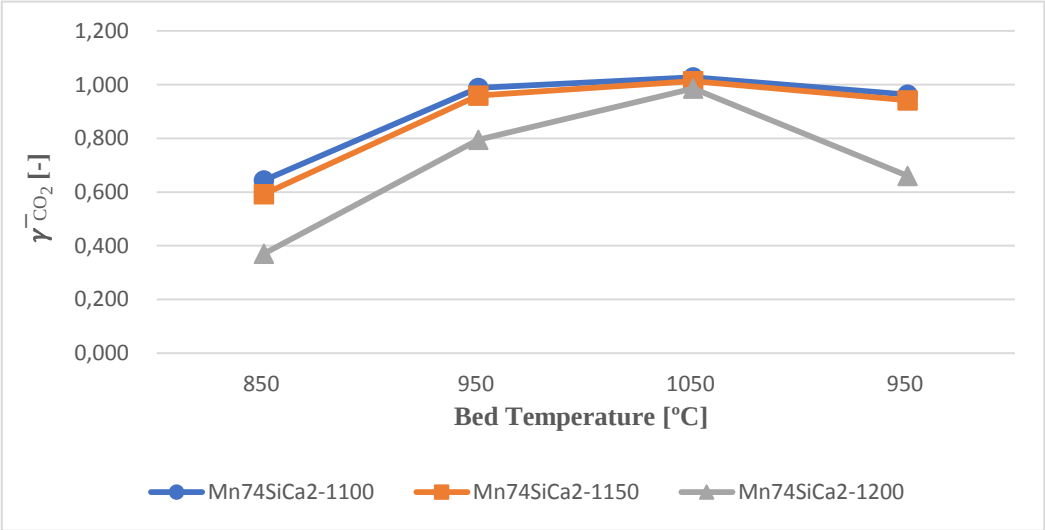
A 27. CO_2 yield as a function of oxygen carrier conversion of methane for Mn74SiCa2 calcined in three temperatures.



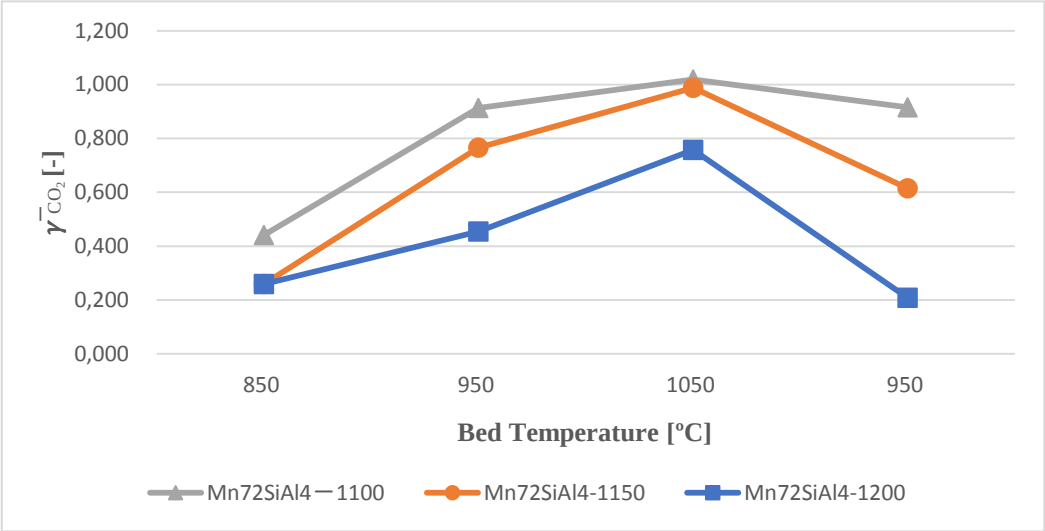
A 28. CO_2 yield as a function of oxygen carrier conversion of methane for Mn74SiAl2 calcined in two temperatures.



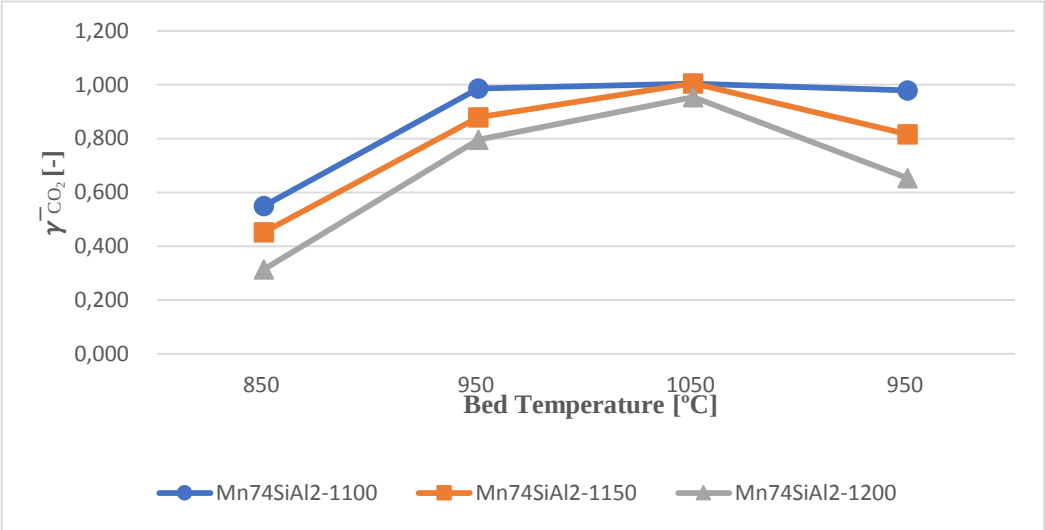
A 29. Average CO_2 yield as a function of oxygen carrier conversion of syngas for Mn71SiCa5 calcined in three temperatures.



A 30. Average CO_2 yield as a function of oxygen carrier conversion of syngas for Mn74SiCa2 calcined in three temperatures.



A 31. Average CO_2 yield as a function of oxygen carrier conversion of syngas for Mn72SiAl4 calcined in two temperatures.



A 32. Average CO_2 yield as a function of oxygen carrier conversion of syngas for Mn74SiAl2 calcined in two temperatures.

6.3 Mechanical durability

B 1. Attrition index of used particles and average CO_2 yield for Mn-Si oxygen carriers supported by CaO.

Oxygen carrier	Attrition index [wt.%/h]	Average CO_2 yield [-]
Mn44SiCa41-1100	7.1	0.874
Mn44SiCa41-1150	51.9	0.686
Mn59SiCa21-1100	4.4	0.886
Mn59SiCa21-1150	18.6	0.821
Mn71SiCa5-1100	2.4	0.915
Mn71SiCa5-1150	25.1	0.909
Mn71SiCa5-1200	0.5	0.662
Mn74SiCa2-1100	23.5	0.988
Mn74SiCa2-1150	117.1	0.959
Mn74SiCa2-1200	1.1	0.795

B 2. Attrition index of used particles and average CO_2 yield for Mn-Si oxygen carriers supported by Al_2O_3.

Oxygen carrier	Attrition index [wt.%/h]	Average CO_2 yield [-]
Mn48SiAl36-1100	1.2	0.185
Mn48SiAl36-1150	0.4	0.227
Mn62SiAl17-1100	6.0	0.889
Mn62SiAl17-1150	3.8	0.722
Mn69SiAl7-1150	0.4	0.755
Mn72SiAl4-1100	2.9	0.913
Mn72SiAl4-1150	5.4	0.766
Mn72SiAl4-1200	0.3	0.454
Mn74SiAl2-1100	5.1	0.986
Mn74SiAl2-1150	3.1	0.879
Mn74SiAl2-1200	0.6	0.796

B 3. Crushing strength of fresh particles and average CO_2 yield for Mn-Si oxygen carriers supported by CaO.

Oxygen carrier	Crushing strength [N]	Average CO_2 yield [-]
Mn44SiCa41-1100	1.0	0.874
Mn44SiCa41-1150	1.5	0.686
Mn59SiCa21-1100	2.0	0.886
Mn59SiCa21-1150	1.6	0.821
Mn71SiCa5-1100	1.6	0.915
Mn71SiCa5-1150	2.1	0.909
Mn71SiCa5-1200	1.6	0.662
Mn74SiCa2-1100	1.6	0.988
Mn74SiCa2-1150	2.1	0.959
Mn74SiCa2-1200	1.6	0.795

B 4. Crushing strength of fresh particles and average CO_2 yield for Mn-Si oxygen carriers supported by Al_2O_3.

Oxygen carrier	Crushing strength [N]	Average CO_2 yield [-]
Mn48SiAl36-1100	0.6	0.185
Mn48SiAl36-1150	1.6	0.227
Mn62SiAl17-1100	0.6	0.889
Mn62SiAl17-1150	1.5	0.722
Mn69SiAl7-1150	0.8	0.755
Mn72SiAl4-1100	0.6	0.913
Mn72SiAl4-1150	1.1	0.766
Mn72SiAl4-1200	2.4	0.454
Mn74SiAl2-1100	0.6	0.986
Mn74SiAl2-1150	1.1	0.879
Mn74SiAl2-1200	1.3	0.796